Paupar LncRNA Promotes KAP1 Dependent Chromatin Changes And Regulates Subventricular Zone Neurogenesis

Ioanna Pavlaki[1#], Farah Alammari[2#], Bin Sun[2], Neil Clark[3], Tamara Sirey[3], Sheena Lee[2], Dan J Woodcock[4], Chris P Ponting[3], Francis G Szele[2] and Keith W Vance[1]*

[1]Department of Biology and Biochemistry, University of Bath, Claverton Down, Bath, BA2 7AY, UK.

[2]Department of Physiology, Anatomy, and Genetics, University of Oxford, South Parks Road, Oxford, OX1 3QX, UK.

[3]MRC Human Genetics Unit, The Institute of Genetics and Molecular Medicine, University of Edinburgh, Western General Hospital, Crewe Road, Edinburgh EH4 2XU.

[4]Warwick Systems Biology Centre, University of Warwick, Coventry, CV4 7AL, UK.

Running title: *Paupar* functionally interacts with KAP1

Character count: 52,993

* Corresponding Author: k.w.vance@bath.ac.uk;

[#] These authors contributed equally to this work

ABSTRACT

Many long non-coding RNAs (lncRNAs) are expressed during central nervous system (CNS) development, yet their *in vivo* roles and molecular mechanisms of action remain poorly understood. *Paupar*, a CNS expressed lncRNA, controls neuroblastoma cell growth by binding and modulating the activity of genome-wide transcriptional regulatory elements. We show here that *Paupar* transcript directly binds KAP1, an essential epigenetic regulatory protein, and thereby regulates the expression of shared target genes important for proliferation and neuronal differentiation. *Paupar* promotes KAP1 chromatin occupancy and H3K9me3 deposition at a subset of distal targets, through formation of a DNA binding ribonucleoprotein complex containing *Paupar*, KAP1 and the PAX6 transcription factor. *Paupar*-KAP1 genome-wide co-occupancy reveals a 4-fold enrichment of overlap between *Paupar* and KAP1 bound sequences. Furthermore, both *Paupar* and Kap1 loss of function *in vivo* accelerates lineage progression in the mouse postnatal subventricular zone (SVZ) stem cell niche and disrupts olfactory bulb neurogenesis. These observations provide important conceptual insights into the *trans*-acting modes of lncRNA-mediated epigenetic regulation, the mechanisms of KAP1 genomic recruitment and identify *Paupar* and *Kap1* as regulators of SVZ neurogenesis.

Keywords: KAP1/lncRNA/neurogenesis/gene regulation/chromatin

INTRODUCTION

A subset of nuclear long noncoding RNAs (lncRNAs) have been shown to act as transcription and chromatin regulators using multiple different regulatory mechanisms. These include local functions close to the sites of lncRNA synthesis (Engreitz, Haines et al., 2016) as well as distal modes of action across multiple chromosomes (Chalei, Sansom et al., 2014, Vance, Sansom et al., 2014). Moreover, lncRNA regulatory effects may be mediated by the act of lncRNA transcription as well as RNA sequence dependent interactions with transcription factors and chromatin regulatory proteins (Rutenberg-Schoenberg, Sexton et al., 2016, Vance & Ponting, 2014). Some lncRNAs have been proposed to act as molecular scaffolds to facilitate the formation of multi-component ribonucleoprotein regulatory complexes (Ilik, Quinn et al., 2013, Maenner, Muller et al., 2013, Tsai, Manor et al., 2010, Yang, Flynn et al., 2014, Zhao, Ohsumi et al., 2010), whilst others may act to guide chromatin regulatory complexes to specific binding sites genome wide (Vance & Ponting, 2014). Studies of *cis*-acting lncRNAs such as *Haunt* and *Hottip* have shown that lncRNA transcript accumulation at their sites of expression can effectively recruit regulatory complexes (Pradeepa, McKenna et al., 2017, Yin, Yan et al., 2015). LncRNAs however have also been reported to directly bind and regulate genes across multiple chromosomes away from their sites of synthesis (Carlson, Quinn et al., 2015, Chalei et al., 2014, Chu, Qu et al., 2011, Vance et al., 2014, West, Davis et al., 2014). By way of contrast, the mechanisms by which such *trans*-acting lncRNAs mediate transcription and chromatin regulation at distal bound target genes are less clear.

LncRNAs show a high propensity to be expressed in brain nuclei and cell types relative to other tissues (Mercer, Dinger et al., 2008, Mercer, Qureshi et al., 2010, Ponjavic, Oliver et al., 2009). The adult neurogenic stem cell-containing mouse subventricular zone (SVZ) contributes to brain repair and can be stimulated to limit damage, but is also a source of tumours (Bardella, Al-Dalahmah et al., 2016, Chang, Adorjan et al., 2016). During SVZ lineage progression GFAP+ neural stem cells (NSC) give rise to Mash1+ and Dlx+ transit amplifying progenitors (TAPs) which in turn generate doublecortin+

63 neuroblasts that migrate to the olfactory bulbs (OB) (Doetsch, Caille et al., 1999). 8,992 lncRNAs are
64 expressed in the SVZ, many of which are differentially expressed during SVZ neurogenesis, suggesting
65 that at least some of these transcripts may play regulatory roles (Ramos, Diaz et al., 2013). However,
66 only a minority of SVZ expressed lncRNAs have been analysed functionally and the full scope of their
67 molecular mechanisms of action remain poorly understood.

68 *Kap1* encodes an essential chromatin regulatory protein that plays a critical role in embryonic
69 development and in adult tissues. Kap1$^{-/-}$ mice die prior to gastrulation while hypomorphic *Kap1*
70 mouse mutants display multiple abnormal embryonic phenotypes, including defects in the
71 development of the nervous system (Cammas, Mark et al., 2000, Herzog, Wendling et al., 2011,
72 Shibata, Blauvelt et al., 2011). KAP1 interacts with chromatin binding proteins such as HP1 and the
73 SETDB1 histone-lysine N-methyltransferase to control heterochromatin formation and to silence gene
74 expression at euchromatic loci (Iyengar & Farnham, 2011). Despite this fundamental role in epigenetic
75 regulation, the mechanisms of KAP1 genomic targeting are not fully understood. KAP1 does not
76 contain a DNA binding domain but was originally identified through its interaction with members of
77 the KRAB zinc finger (KRAB-ZNF) transcription factor family. Subsequent studies however revealed that
78 KRAB-ZNF interactions cannot account for all KAP1 genomic recruitment events. KAP1 preferentially
79 localises to the 3' end of zinc finger genes as well as to many promoters and intergenic regions in
80 human neuronal precursor cells. A mutant KAP1 protein however that is unable to interact with KRAB-
81 ZNFs still binds to promoters suggesting functionally distinct subdomains (Iyengar, Ivanov et al., 2011).
82 This work points to the presence of alternative, KRAB-ZNF independent mechanisms that operate to
83 target KAP1 to a distinct set of genomic binding sites. We reasoned that this may involve specific RNA-
84 protein interactions between KAP1 and chromatin bound lncRNAs.

85 The CNS expressed intergenic lncRNA *Paupar* represents an ideal candidate chromatin-enriched
86 lncRNA with which to further define *trans*-acting mechanisms of lncRNA mediated gene and chromatin
87 regulation. *Paupar* is transcribed upstream from the *Pax6* transcription factor gene and acts to control

proliferation and differentiation of N2A neuroblastoma cells *in vitro* (Vance et al., 2014). *Paupar* regulates *Pax6* expression locally, physically associates with PAX6 protein and interacts with distal transcriptional regulatory elements to control gene expression on multiple chromosomes in N2A cells in a dose-dependent manner. Here, we show that *Paupar* directly interacts with KAP1 in N2A cells and that together they control the expression of a shared set of target genes enriched for regulators of neural proliferation and differentiation. Our findings indicate that *Paupar*, KAP1 and PAX6 physically associate on chromatin within the regulatory region of shared target genes and that *Paupar* knockdown reduces both KAP1 chromatin association and histone H3 lysine 9 tri-methylation (H3K9me3) at PAX6 co-bound locations. Genome-wide occupancy maps further identified a preferential enrichment in the overlap between *Paupar* and KAP1 binding sites on chromatin. Our results also show that both *Paupar* and KAP1 loss of function *in vivo* accelerates lineage progression in the mouse postnatal SVZ stem cell niche and disrupts olfactory bulb neurogenesis. We propose that *Paupar* and Kap1 are novel regulators of SVZ neurogenesis, and that *Paupar* operates as a transcriptional cofactor to promote KAP1 dependent chromatin changes at a subset of bound regulatory elements in *trans* via association with non-KRAB-ZNF transcription factors such as PAX6.

RESULTS

Paupar directly binds the KAP1 chromatin regulatory protein in mouse neural cells in culture

The lncRNA *Paupar* binds transcriptional regulatory elements across multiple chromosomes to control the expression of distal target genes in N2A neuroblastoma cells (Vance et al., 2014). Association with transcription factors such as PAX6 assist in targeting *Paupar* to chromatin sites across the genome. As *Paupar* depletion does not alter PAX6 chromatin occupancy (Vance et al., 2014) we hypothesized that *Paupar* may recruit transcriptional cofactors to PAX6 and other neural transcription factors to regulate gene expression. To test this, we sought to identify transcription and chromatin regulatory proteins that bind both *Paupar* and PAX6 in N2A cells in culture. *In vitro* transcribed biotinylated *Paupar* was therefore immobilised on streptavidin beads and incubated with N2A cell nuclear extract in a pull down assay. Bound proteins were washed, eluted and identified using mass spectrometry (Fig 1a). This identified a set of 78 new candidate *Paupar*-associated proteins that do not bind a control RNA of similar size, including 28 proteins with annotated functions in the control of gene expression that might function as transcriptional cofactors (Fig 1b and Supplemental Table S1).

We next performed native RNA-IP experiments in N2A cells to validate potential associations between the endogenous *Paupar* transcript and five gene expression regulators. These were: RCOR3, a member of the CoREST family of proteins that interact with the REST transcription factor; KAP1, a key epigenetic regulator of gene expression and chromatin structure; PPAN, a previously identified regulator of *Pax6* expression in the developing eye; CHE-1, a polymerase II interacting protein that functions to promote cellular proliferation and block apoptosis; and ERH, a transcriptional cofactor that is highly expressed in the eye, brain and spinal cord.

The results revealed that the *Paupar* transcript, but not a non-specific control RNA, was >2-fold enriched using antibodies against RCOR3, KAP1, ERH, PPAN or CHE1 compared to an IgG isotype

control in a native RNA-IP experiment (Fig 1c). In addition, *Paupar* did not associate above background with SUZ12, EED and EZH2 Polycomb proteins used as negative controls. This served to further confirm the specificity of the *Paupar* lncRNA-protein interactions because Polycomb proteins associate with a large number of RNAs (Davidovich, Wang et al., 2015) and yet were not identified as *Paupar* interacting proteins in our pull down assay. The endogenous *Paupar* transcript therefore associates with proteins involved in transcription and chromatin regulation in proliferating N2A cells.

To characterise *Paupar* lncRNA-protein interactions further we used UV-RNA-IP to test whether *Paupar* interacts directly with any of these five cofactors. These data showed that *Paupar*, but not an *U1snRNA* control, is highly enriched using antibodies against KAP1 or RCOR3 compared to an IgG control (Fig 1d). A lower level of *Paupar* enrichment is found with CHE1 whereas ERH or PPAN do not appear to interact directly with *Paupar* (Supplemental Fig S1a). Furthermore, the association of *Paupar* with both KAP1 and RCOR3 was reduced in the absence of UV treatment (Fig 1e). These results therefore indicate that the endogenous *Paupar* transcript directly and specifically associates with RCOR3 and KAP1 transcriptional cofactors in neural precursor-like cells in culture.

As a first step to determine whether KAP1 or RCOR3 can act as PAX6 associated transcriptional cofactors we performed immunoprecipitation experiments in N2A cells using transfected FLAG-tagged PAX6 and with HA-KAP1 or HA-RCOR3 proteins. Immunoprecipitation of FLAG-tagged PAX6 using anti-FLAG beads co-immunoprecipitated transfected KAP1 protein, but not RCOR3 (Fig 1f), suggesting that PAX6 and KAP1 are present within the same multi-component regulatory complex. Consistent with this, a previous study showed that KAP1 interacts with PAX3 through the amino terminal paired domain, which is structurally similar in PAX6, to mediate PAX3 dependent transcriptional repression (Hsieh, Yao et al., 2006). Together, these results indicate that KAP1 may regulate *Paupar* and PAX6 mediated gene expression programmes.

Paupar and KAP1 control expression of a shared set of target genes that are enriched for regulators of neuronal function and cell cycle in N2A cells

KAP1 regulates the expression of genes involved in the self-renewal and differentiation of multiple cell types, including neuronal cells (Iyengar & Farnham, 2011) and thus is an excellent candidate interactor for mediating the transcriptional regulatory function of *Paupar*. To investigate whether *Paupar* and KAP1 functionally interact to control gene expression we first tested whether they regulate a common set of target genes. We depleted *Kap1* expression in N2A cells using shRNA transfection and achieved approximately 90% reduction in both protein (Fig 2a) and transcript (Fig 2b) levels. *Paupar* levels do not change upon KAP1 knockdown indicating that KAP1 dependent changes in gene expression are not due to regulation of *Paupar* expression (Fig 2b). Transcriptome profiling using microarrays then identified 1,913 differentially expressed genes whose expression significantly changed (at a 5% false discovery rate [FDR]) greater than 1.4-fold (log2 fold change ≈ 0.5) upon KAP1 depletion (Fig 2c and Supplemental Table S2). 282 of these genes were previously identified to be regulated by human KAP1 in Ntera2 undifferentiated human neural progenitor cells (Iyengar et al., 2011). Transient reduction of *Kap1* expression by approximately 55% using a second shRNA expression vector (*Kap1* shB) also induced expression changes for 7 out of 8 *Kap1* target genes with known functions in neuronal cells that were identified in the microarray (Supplemental Fig 1b). These data further validate the specificity of the KAP1 regulated gene set.

We previously showed that *Paupar* knockdown induces changes in the expression of 942 genes in N2A cells (Vance et al., 2014). Examination of the intersection of KAP1 and *Paupar* transcriptional targets identified 244 genes whose levels are affected by both *Paupar* and KAP1 knockdown in this cell type (Fig 2d and Supplemental Table S3). This represents a significant 3.6-fold enrichment over the number expected by random sampling and is not due to co-regulation because *Kap1* is not a *Paupar* target (Vance et al., 2014). A large majority (87%; 212/244) of these common targets are positively regulated by *Paupar* and for two-thirds of these genes (161/244) their expression changes in the same direction upon *Paupar* or KAP1 knockdown (Fig 2e). Furthermore, Gene Ontology enrichment analysis of these 244 genes showed that *Paupar* and KAP1 both regulate a shared set of target genes enriched for regulators of interphase, components of receptor tyrosine kinase signalling

pathways as well as genes involved in nervous system development and essential neuronal cell functions such as synaptic transmission (Fig 2f). Genes targeted by both *Paupar* and KAP1 are thus expected to contribute to the control of neural stem-cell self-renewal and neural differentiation.

***Paupar*, KAP1 and PAX6 associate on chromatin within the regulatory region of shared target genes**

In order to investigate *Paupar* mediated mechanisms of distal gene regulation we next sought to determine whether *Paupar,* KAP1 and PAX6 can form a ternary complex on chromatin within the regulatory regions of their shared target genes. To do this, we first integrated our analysis of PAX6 regulated gene expression programmes in N2A cells (Vance et al., 2014) and identified 87 of the 244 *Paupar* and KAP1 common targets, which is 35.8-fold greater than expected by random sampling, whose expression is also controlled by PAX6 (Fig 3a and Supplemental Table S3). We found that 34 of these genes contain a CHART-Seq mapped *Paupar* binding site within their GREAT defined putative regulatory regions (Vance, 2016, Vance et al., 2014) and predicted that these represent functional *Paupar* binding events within close genomic proximity to direct transcriptional target genes (Fig 3a and Supplemental Table S3).

ChIP-qPCR analysis previously identified four of these *Paupar* bound locations within the regulatory regions of the *Mab21L2*, *Mst1*, *E2f2* and *Igfbp5* genes that are also bound by PAX6 in N2A cells (Vance et al., 2014). We therefore measured KAP1 chromatin occupancy at these regions as well as at a negative control sequence within the first intron of *E2f2* using ChIP and identified a specific enrichment of KAP1 chromatin association at the *Mab21L2*, *Mst1*, *E2f2* and *Igfbp5* genes compared to an IgG isotype control (Fig 3b). KAP1 binding to these regions is only 2- to 4-fold reduced compared to the Zfp382 3' UTR positive control (Fig. 3b) which represents an exemplar high affinity KAP1 binding site (Iyengar et al., 2011). Furthermore, KAP1 and *Paupar* also co-occupy a binding site within the *Ezh2* gene. As *Ezh2* is regulated by *Paupar* and KAP1 but not by PAX6 this suggests that *Paupar* and KAP1 can also interact with specific sites on chromatin using additional PAX6

202 independent mechanisms. Together, these data suggest that *Mab21L2*, *Mst1*, *E2f2* and *Igfbp5* are co-
203 ordinately regulated by a ribonucleoprotein complex containing *Paupar*-KAP1-PAX6.

204 **_Paupar_ functions as a transcriptional cofactor to promote KAP1 chromatin occupancy and**
205 **H3K9me3 deposition at PAX6 bound sequences**

206 KAP1 is recruited to its target sites within 3'UTRs of ZNF genes through the association with KRAB-ZNF
207 transcription factors (Iyengar et al., 2011, O'Geen, Squazzo et al., 2007). However, *Paupar* bound
208 sequences are preferentially located at gene promoters and are not enriched for KRAB-ZNF
209 transcription factor binding motifs (Vance et al., 2014). This suggests that *Paupar* may play a role in
210 recruiting KAP1 to a separate class of binding site in a KRAB-ZNF independent manner. To test this,
211 *Paupar* expression was first depleted using transient transfection of *Paupar* targeting shRNA
212 expression vectors (Fig 3c). We then performed ChIP-qPCR to measure KAP1 chromatin occupancy in
213 control and *Paupar* knockdown N2A cells at the four *Paupar*-KAP1-PAX6 co-occupied binding sites
214 within the regulatory regions of the *Mab21L2*, *Mst1*, *E2f2* and *Igfbp5* genes, a *Paupar*-KAP1 bound
215 sequence within the *Ezh2* gene that is not regulated by PAX6, and a control sequence that is not
216 bound by *Paupar*. The results show that KAP1 chromatin binding is significantly decreased at the four
217 *Paupar*-KAP1-PAX6 bound regions upon *Paupar* depletion and that the extent of KAP1 chromatin
218 association appears to be dependent on *Paupar* transcript levels (Fig. 3d). KAP1 chromatin association
219 is also not reduced at the *Ezh2* gene *Paupar*-KAP1 binding site or at the control sequence that is not
220 bound by *Paupar* (Fig 3d), whilst total KAP1 protein levels do not detectably change upon *Paupar*
221 knockdown (Fig 3e), further confirming specificity.

222 These results imply that *Paupar* functions to promote KAP1 chromatin association at a subset of its
223 genomic binding sites in *trans* and that this requires the formation of a DNA bound ternary complex
224 containing *Paupar*, KAP1 and PAX6. Consistent with this, co-expression of the *Paupar* lncRNA
225 promotes KAP1-PAX6 association in a dose dependent manner in an immunoprecipitation
226 experiment (Fig 3f). This effect is specific for the *Paupar* transcript because expression of a size-

matched control RNA does not alter KAP1-PAX6 association. *Paupar* thus functions as a transcriptional cofactor to promote the assembly of a *Paupar*-KAP1-PAX6 ternary complex on chromatin in *trans*. This ribonucleoprotein complex appears to function as a regulator of genes involved in controlling neural stem cell self-renewal and differentiation.

We next tested whether *Paupar* can induce histone modification changes at bound target genes on different chromosomes away from its sites of synthesis. As KAP1 interacts with the SETDB1 methyltransferase to mediate histone H3K9me3 deposition (Schultz, Ayyanathan et al., 2002), we first determined the levels of H3K9me3 at *Mab21L2*, *Mst1*, *E2f2* and *Igfbp5* bound sequences using ChIP-qPCR. This revealed an enrichment of H3K9me3 modified chromatin at all five locations (Supplemental Fig S2), consistent with a previous study showing that many KAP1 bound promoters are marked by H3K9me3 (O'Geen et al., 2007). shRNA mediated reduction of *Paupar* transcript levels using two different shRNAs resulted in a significant decrease in histone H3K9me3 modification at 3 of 4 of these shared binding sites tested using ChIP (Fig. 3g, h). No change in histone H3K9me3 was detected at *Ezh2* gene whose expression does not change upon PAX6 depletion. Together, these data show that *Paupar* functions to modulate KAP1 chromatin association and histone H3K9me3 deposition at a subset of its shared binding sites in *trans*.

Paupar co-occupies an enriched subset of KAP1 binding sites genome-wide

We next examined the intersection between *Paupar* and KAP1 bound locations genome-wide in order to generate a more comprehensive view of the potential of *Paupar* for regulating KAP1 function. ChIP-seq profiling of KAP1 chromatin occupancy showed that KAP1 associates with 5510 genomic locations compared to input DNA in N2A cells (1% FDR) (Supplemental Table S4). KAP1 binding sites are particularly enriched at promoter regions, over gene bodies and at the 3'UTRs of zinc finger genes (Fig. 4a), consistent with previous studies mapping human KAP1 genomic occupancy (Iyengar et al., 2011, O'Geen et al., 2007). Intersection of KAP1 bound locations with our CHART-seq map of *Paupar* genomic binding in N2A cells (Vance et al., 2014) identified 46 KAP1 binding sites that

252 are co-occupied by *Paupar* and not bound in a LacZ negative control CHART-seq pull down (Fig. 4b),
253 only one of which is located within the 3'UTR of a ZNF gene (zfp68) (Supplemental Table S4). Notably,
254 this represents a significant ($p < 0.001$) 4-fold enrichment of *Paupar* and KAP1 co-occupied locations
255 as estimated using Genome Association Tester (GAT) (Fig. 4b). In addition, plotting the distribution of
256 peak intensities across these co-occupied regions revealed a precise coincidence of *Paupar* and KAP1
257 binding (Fig. 4c). These data therefore show that *Paupar* co-occupies an enriched subset of KAP1
258 bound sequences genome-wide and suggest that *Paupar* mediated genomic recruitment of KAP1
259 may involve interactions with other transcription factors in addition to KRAB-ZNF association.

260 **_Paupar_ and Kap1 regulate the SVZ neurogenic niche and olfactory bulb neurogenesis**

261 Our results indicate that *Paupar* and KAP1 regulate the expression of shared target genes important
262 for proliferation and neuronal differentiation in N2A cells. We next expanded this observation and
263 tested whether *Paupar* and Kap1 can regulate the same neurodevelopmental process *in vivo*. To do
264 this, we used the mouse SVZ system as it is experimentally convenient for discovering many different
265 neurodevelopmental mechanisms. Lineage progression can be monitored by electroporating the
266 neonatal SVZ; in 24 hrs the NSC are labelled, 3 days post electroporation (3dpe) TAPs appear and by 7
267 dpe labelled neuroblasts are seen migrating into the OB (Boutin, Diestel et al., 2008a, Chesler, Le
268 Pichon et al., 2008).

269 We first showed using RT-qPCR that *Paupar* is expressed in the SVZ, as well as in neurospheres
270 cultured from P4 SVZ (Supplemental Fig S3a), and then confirmed the efficiency of the *Paupar*
271 targeting shRNA expression vectors to deplete *Paupar* transcript in neurospheres cultured from P4 SVZ
272 (Supplemental Fig S3b). sh165 caused robust *Paupar* knockdown (KD) whereas sh408 moderately
273 reduced *Paupar* expression enabling us to identify dose dependent regulatory effects. Nucleofection
274 of *Paupar* KD constructs and a scrambled (scr) control plasmid targeted ~60% of cells, as measured
275 using GFP, but we determined *Paupar* levels in all cells. Thus on a cell-by-cell basis the relative level of
276 knockdown is predicted to be greater than shown (Supplemental Fig S3b). To study *Paupar* function in

277 neurogenesis, we electroporated P1 pups with *Paupar* KD constructs or scr controls and examined the
278 SVZ 24 hours post electroporation (24hpe) and 3 days post electroporation (3dpe). To control for
279 differences in the number of cells electroporated in the different groups we measured the percentage
280 of GFP+ cells expressing lineage markers (Fig. 5a, c). Immunostaining showed that at 24hpe, the
281 percent of GFP+ cells expressing the TAP marker MASH1 was increased by more than 50% with sh165
282 knockdown (Fig. 5b). This was confirmed by immunostaining with the TAP and neuroblast marker DLX2
283 which showed a greater than 30% increase with both knockdown constructs (Fig. 5b). Additionally we
284 showed that the percentage of GFP+ cells positive for the proliferation marker Ki67 was significantly
285 increased in the sh165 group (Fig. 5b). At 24hpe the majority of cells in scramble controls are radial
286 glia-like neural stem cells (Boutin et al., 2008a, Chesler et al., 2008). These results thus suggest that
287 after *Paupar* KD a larger percentage of cells are progressing into the next phase of the SVZ lineage and
288 are actively proliferating. We next carried out immunohistochemistry for the same markers at 3dpe
289 and quantification showed that fewer GFP+ cells expressed the radial glial/neural stem cell marker
290 GFAP upon KD with the sh165 construct (Fig. 5c-e). This further suggests that *Paupar* loss increases
291 lineage progression and/or diminishes SVZ stem cell maintenance.

292 The Allen Brain Atlas shows *Kap1* expression in the SVZ. To study the functional effect of *Kap1* on SVZ
293 neurogenesis, P1 pups were electroporated with either a scr control or the *Kap1* shRNA expression
294 vectors that we used to deplete *Paupar* in N2A cells (Fig. 3 and Supplemental Fig S1b) and sections
295 were immunostained for GFP and SVZ markers (Fig. 5f). At 3dpe of *Kap1* shA and shB, the percentage
296 of GFP+ cells that expressed the radial glial/neural stem cell marker GFAP significantly decreased (Fig.
297 5g). This is similar to *Paupar* KD and is consistent with accelerated lineage progression. Also similar to
298 *Paupar* KD at 3dpe, *Kap1* KD did not alter the percent of GFP+ cells which expressed DLX2 or Ki67.
299 However, the percentage of MASH1+ cells decreased slightly but significantly at 3dpe post *Kap1* shA
300 KD, which was not found upon *Paupar* KD. Since we showed that *Paupar* and *Kap1* regulate similar as
301 well as different genes this result may be due to differential gene regulation. Furthermore, these
302 *Paupar* and *Kap1* mediated changes in cell subtype numbers are not due to altered rates of cell death

303 because we did not detect changes in the number of CASPASE3+ cells (Supplemental Fig S4a), or in the
304 percentage of GFP+ cells that are Tunel+ between scr control and any of the *Paupar* or *Kap1* shRNA
305 expression vectors (Supplemental Fig S4b, c).

306 We next studied how *Paupar* or *Kap1* affects the number of electroporated cells that reach the OB
307 7dpe. There were significantly fewer GFP+ cells in the OB after *Paupar* KD using sh165 KD compared to
308 the scr control whilst KD with sh408 caused a slight but statistically non-significant decrease in OB
309 GFP+ cell numbers (Fig. 6a, b). Co-staining with the immature neuroblast marker DCX (Yang,
310 Sundholm-Peters et al., 2004) showed that all GFP+ cells in the OB were DCX+ and this was not altered
311 by *Paupar* KD (Supplemental Fig S3d). Similar to *Paupar*, at 7dpe of either Kap1 KD construct, there
312 was a significant reduction in the number of GFP+ cells that had migrated from the SVZ to the OB (Fig.
313 6c, d). These results suggest that both *Paupar* and *Kap1* are required for the production of newborn
314 OB neurons.

315 Interestingly, *Paupar* as well as *Kap1* knockdown altered the morphology of newborn neurons that
316 migrated to the OB (Fig. 6e-h). In scr controls many GFP+ neurons in the OB granule layer had
317 processes extending radially towards the pial surface and some of the processes were branched and
318 these were classified as class I cells (Fig 6e, f). By contrast, after *Paupar* KD, a variety of abnormal
319 morphologies were observed, which we classified as class II or class III (Fig 6e). Class II cells were rare
320 but were distinguished by many short branched processes. Class III cells were stunted with only short
321 or no processes (Fig 6e). Quantification revealed that after *Paupar* KD the percentage of cells with
322 Class I morphology was 34±2% in scr controls but only 8±3% in sh165 and 6±3% in sh408 (P=0.0005
323 and P=0.0009, respectively) (Fig. 6g). Conversely, after *Paupar* KD there were more class III neurons in
324 the sh165 group 87±4% as well as in the sh408 group 85±6% compared to 58±5% controls (P=0.003
325 and P=0.02, respectively). *Kap1* knockdown showed similar effects (Fig 6f, h); shA and shB resulted in
326 16.7±5.6% and 19.3±2.0% of Class I neurons versus 42.0±1.5% in controls (P=0.012 and P=0.013,
327 respectively). Again, the number of Class III neurons increased from 54.7±2.2% in controls to

328 81.3±5.6% after shA KD and 77.3±0.3% after shB KD (P=0.0009 and P=0.0005, respectively). These data
329 further suggest that *Kap1* and *Paupar* affect postnatal neurogenesis by disrupting both migration into
330 the OB and the morphology of newborn neurons.

331

DISCUSSION

LncRNAs can bind and regulate target genes on multiple chromosomes away from their sites of transcription. Furthermore, the number of lncRNAs that function in this way is steadily increasing suggesting that nuclear lncRNAs are likely to exert a wide range of currently uncharacterised, *trans*-acting functions in transcription and chromatin regulation. Moreover, loss-of-function studies using animal model systems are needed to identify and characterise lncRNA regulatory roles during embryonic development and in adult tissue homeostasis to clarify the importance of this class of transcript *in vivo*.

To gain novel insights into lncRNA gene regulation we investigated the mode of action of the CNS expressed lncRNA *Paupar* at chromosomal binding sites away from its site of synthesis in N2A cells. We show that *Paupar* directly binds the KAP1 epigenetic regulatory protein and thereby regulates the expression of shared target genes important for proliferation and neuronal differentiation. Our data indicate that *Paupar* modulates histone H3K9me deposition at a subset of distal bound transcriptional regulatory elements through its association with KAP1, including at a binding site upstream of the *E2f2* gene. These chromatin changes are consistent with our previous report that this *E2f2* bound sequence functions as a transcriptional enhancer whose activity is restricted by *Paupar* transcript levels (Vance et al., 2014). Our results therefore suggest a model in which *Paupar* directed histone modification changes in *trans* alter the activity of bound regulatory elements in a dose dependent manner.

Several other lncRNAs have also been shown to alter the chromatin structure of target genes in *trans*. These include the human *PAUPAR* orthologue which can inhibit H3K4 tri-methylation of the *Hes1* promoter in eye cancer cell lines, as well as lncRNA-HIT which induces p100/CBP mediated changes in histone H3K27ac at bound sequences to regulate genes involved in chondrogenesis (Carlson et al., 2015, Ding, Wang et al., 2016). The lncRNA *Hotair* is one of the most studied *trans*-acting lncRNAs. Whilst *Hotair* has been proposed to guide PRC2 to specific locations in the genome to induce H3K27me3 and silence gene expression (Chu et al., 2011), recent conflicting studies report that PRC2

357 associates with low specificity to lncRNAs and suggest that *HOTAIR* does not directly recruit PRC2 to
358 the genome to silence gene transcription (Davidovich et al., 2015, Kaneko, Son et al., 2013, Portoso,
359 Ragazzini et al., 2017). Mechanistic studies on individual *trans*-acting lncRNAs such as *Paupar* are
360 therefore needed to further define general principles of genome-wide lncRNA transcription and
361 chromatin regulation.

362 It is proposed that lncRNAs may guide chromatin modifying complexes to distal regions in the genome
363 though RNA-RNA associations at transcribed loci, or either directly through RNA-DNA base pairing or
364 indirectly through RNA-protein-DNA associations (Rutenberg-Schoenberg et al., 2016, Vance &
365 Ponting, 2014). We show that *Paupar* acts to increase KAP1 chromatin association by promoting the
366 formation of a DNA binding regulatory complex containing *Paupar*, KAP1 and PAX6 within the
367 regulatory regions of shared target genes in *trans*, as illustrated in the model in Fig 7. This suggests
368 that *Paupar* functions as a cofactor for transcription factors such as PAX6 to modulate target gene
369 expression across multiple chromosomes. In a similar manner, *Prncr1* and *Pcgem1* lncRNAs interact
370 with the androgen receptor (AR) and associate with non-DNA binding cofactors to facilitate AR
371 mediated gene regulation (Yang, Lin et al., 2013). LncRNA mediated recruitment of chromatin
372 regulatory proteins to DNA bound transcription factors may represent a common mechanism of *trans*-
373 acting lncRNA gene regulation, in line with their suggested role as molecular scaffolds (Tsai et al.,
374 2010).

375 KAP1 is guided to 3'UTR of zinc finger genes in the genome through association with KRAB-ZNF
376 transcription factors (O'Geen et al., 2007). However, the mechanisms of KAP1 genome-wide
377 recruitment are not fully understood (Iyengar et al., 2011). Our data identify KAP1 as a novel RNA
378 binding protein and show that *Paupar* plays a role in modulating the recruitment of KAP1 to specific
379 PAX6 bound locations in the genome. We further assessed the extent to which *Paupar* may be able
380 to modulate KAP1 genome-wide recruitment and identified 46 shared binding sites on chromatin,
381 only one of which was within a 3' UTR of a zinc finger gene. These results raise the possibility that

382 additional chromatin enriched lncRNAs may operate to recruit KAP1 to specific locations in the
383 genome and that this may involve context specific interactions with both KRAB-ZNF as well as non
384 KRAB-ZNF containing transcription factors such as PAX6.

385 Our knockdown studies indicate that *Paupar* and *Kap1* are required for normal postnatal SVZ
386 neurogenesis *in vivo*. Neonatal SVZ stem cells are the cells lining the ventricles postnatally and are
387 thus are initially targeted by electroporation with TAPs appearing after 3 days and neuroblasts after
388 one week (Boutin et al., 2008a, Chesler et al., 2008). Reduced *Paupar* expression increased
389 proliferation in stem cells suggesting it normally maintains stem cell quiescence and restricts lineage
390 progression. Supporting this, the TAP markers MASH1 and DLX2 increased one day after *Paupar* KD.
391 Importantly, *Mash1* is necessary for stem cell activation (Andersen, Urban et al., 2014) and
392 maintaining neurogenic proliferation (Castro, Martynoga et al., 2011). Similarly, *Dlx2* is necessary for
393 SVZ neurogenesis (Brill, Snapyan et al., 2008) and stimulates lineage progression (Suh, Obernier et al.,
394 2009). Therefore, increased MASH1 and DLX2 levels after *Paupar* KD likely accelerate lineage
395 progression. *Gfap* expression is precipitously lost as neonatal SVZ stem cells transition to TAPS
396 (Doetsch, Garcia-Verdugo et al., 1997). Three days after *Paupar* knockdown GFAP decreased, further
397 suggesting that *Paupar* negatively regulates lineage progression. Similarly, *Kap1* knockdown
398 decreased *Gfap* expression, suggesting *Paupar* and *Kap1* may have other SVZ functions in common.
399 However, *Kap1* but not *Paupar* KD decreased MASH1 levels 3dpe possibly due to the fact that they
400 regulate common as well as distinct programmes of gene expression. Both *Paupar* and *Kap1* loss-of-
401 function reduced the number newborn neurons in the OB. Accelerated lineage progression does not
402 predict reduced OB neurogenesis and the SVZ effects may not be directly linked the OB effects. We
403 controlled for apoptosis and showed that neither *Paupar* nor *Kap1* seems to regulate apoptosis in
404 the SVZ neurogenic system. However, fewer newborn neuroblasts had healthy morphology and more
405 had stunted morphology after *Paupar* or *Kap1* knockdown.

406 This study identifies *Paupar* and *Kap1* as novel regulators of SVZ neurogenesis *in vivo* and provides
407 important conceptual insights into the distal modes of lncRNA mediated gene regulation. Given the
408 widespread role played by *Kap1* in genome regulation and chromatin organisation we anticipate that
409 further chromatin associated lncRNAs will be found to functionally interact with KAP1.

410

MATERIALS AND METHODS

Plasmid Construction

Kap1 targeting short hairpin RNAs (shRNAs), designed using the Whitehead Institute siRNA selection program, were synthesized as double stranded DNA oligonucleotides and ligated into pBS-U6-CMVeGFP as shown previously (Vance et al., 2014). The *Paupar* targeting sh165 and sh408 expression constructs, the non-targeting scrambled control shRNA and pCAGGS-*Paupar* expression vector are also detailed in (Vance et al., 2014). To generate the PAX6 expression vector, *Pax6* coding sequence was PCR amplified from mouse N2A cell cDNA as a NotI-XhoI fragment and inserted into pcDNA3.1(+) (Invitrogen). The forward primer incorporated a DNA sequence to insert the DYKDDDDK FLAG epitope tag in frame at the amino terminal end of PAX6. *Rcor3* coding sequence was also PCR amplified from mouse N2A cell cDNA and cloned into pcDNA3.1(+) to generate pcDNA-RCOR3. pcDNA3-HA-KAP1 was a kind gift from Colin Goding (Ludwig Institute, Oxford). The sequences of the oligonucleotides used in this study are listed in Supplemental Table S5.

Cell Culture

N2A mouse neuroblastoma cells (ATCC CCL-131) were grown in DMEM supplemented with 10% foetal bovine serum. All transfections were performed using FuGENE 6 (Promega) following the manufacturer's instructions. To generate *Kap1* knockdown cells, approximately 2×10^5 cells were plated per well in a six well plate. 16–24 h later cells were transfected with 1.5 μg *Kap1* shRNA expression construct and 300 ng (5:1 ratio) pTK-Hyg (Clontech). Three days after transfection, cells were trypsinised, resuspended in growth medium containing 200 μg/ml Hygromycin B and plated onto a 6 cm dish. Drug resistant cells were grown for 7 days and harvested as a pool.

Immunoprecipitation

1×10^6 N2A cells were seeded per 10 cm dish. The next day, cells were transfected with different combinations of pcDNA3-FLAG-PAX6, pcDNA3-Myc-KAP1, pCAGGS-Paupar, pCAGGS-AK034351

control transcript or pcDNA3.1 empty vector. 6 μg plasmid DNA was transfected in total. Two days later, cells were washed twice with ice-cold PBS, transferred to 1.5 ml microcentrifuge tubes and lysed in 1 ml ice-cold IP Buffer (IPB) (50 mM Hepes pH 7.5, 350 mM NaCl, 1 mM $MgCl_2$, 0.5 mM EDTA and 0.4% IGEPAL CA-630) for 30 min, 4°C with rotation. Lysates were pelleted at 14,000 rpm, 20 min, 4°C in a microfuge, supernatant was added to 30 μl anti-FLAG M2 Magnetic Beads (#M8823, Sigma) and incubated overnight at 4°C with rotation. Beads were washed three times with IPB and eluted in 20 μl Laemmli sample buffer for 5 min at 95°C. Bound proteins were detected by Western Blotting using anti-FLAG M2 (F3165, Sigma), anti-KAP1 (ab10483, Abcam), anti-RCOR3 (A301-273A, Bethyl Laboratories) and Protein A HRP (ab7456, Abcam).

RNA Pull Down Assay

Sense RNA was *in vitro* transcribed from pCR4-TOPO-*Paupar* using T7 RNA polymerase, according to manufacturer's instructions (New England Biolabs). Transcribed RNA was concentrated and purified using the RNeasy MinElute Cleanup kit (Qiagen). Purified RNA was then 5' end labelled with biotin-maleimide using a 5' EndTag nucleic acid labelling system (Vector laboratories). Streptavidin coated Dynabeads M-280 (Invitrogen) were washed, prepared for RNA manipulation and the 5' biotinylated RNA bound according to manufacturer's instructions. N2A cell nuclear extract was diluted in affinity binding/washing buffer (150 mM NaCl, 50 mM HEPES, pH 8.0, 0.5% Igepal, 10 mM $MgCl_2$) in the presence of 100ug/ml tRNA, 40U/ml RNaseOUT (Invitrogen) and a protease inhibitor cocktail (Roche). RNA coated beads were incubated with nuclear extract at room temperature for 2 hours with rotation. The supernatant was then removed, the beads washed six times (10 min) with affinity/binding washing buffer, and bound protein eluted by heating to 95°C in the presence of Laemmli sample buffer for 5 min. Samples were loaded onto a 10% Tris-glycine polyacrylamide gel (BioRad) and subjected to denaturing SDS-PAGE until they just entered the resolving gel. Protein samples were then excised, diced, and washed three times with nanopure water. Tryptic digest and mass

spectrometry were performed by the Central Proteomics Facility (Dunn School of Pathology, University of Oxford).

RNA-IP

Approximately $1x10^7$ N2A cells were used per RNA-IP. Native RNA-IP experiments were performed using the Magna RIP Kit (Millipore) according to the manufacturer's instructions. UV-RIP was carried out as described in (Vance et al., 2014). We used the following rabbit polyclonal antibodies: anti-RCOR3 (A301-273A, Bethyl Laboratories), anti-CoREST (07-455, Millipore), anti-KAP1 (ab10483, Abcam), anti-ERH (ab96130, Abcam), anti-PPAN (11006-1-AP, Proteintech Group) and rabbit IgG (PP64B, Millipore).

Chromatin Immunoprecipitation

4×10^6 N2A cells per ChIP were seeded in 15 cm plates. The next day, cells were transfected with either 15 μg *Paupar* targeting shRNA expression vectors or a non-targeting scr control. Three days later cells were harvested for ChIP using either 5 μg anti-KAP1 (ab10483, Abcam), anti-histone H3K9me3 (39161, Active Motif) or normal rabbit control IgG (#2729, Cell Signalling Technology) antibodies. ChIP was performed as described in (Vance et al., 2014). For KAP1 ChIP-seq the following modifications were made to the protocol: approximately $2x10^7$ N2A cells per ChIP were double cross-linked, first using 2 mM disuccinimidyl glutarate (DSG) for 45 min at room temperature, followed by 1% formaldehyde for 15 min at room temperature, as described in (Nowak, Tian et al., 2005). Chromatin was sheared to approximately 200 bp using a Bioruptor Pico (Diagenode) and ChIP DNA and matched input DNA from two independent KAP1 ChIP experiments were sequenced on an Illumina HiSeq 4000 (150 bp paired-end sequencing).

ChIP-seq Analysis

The Babraham Bioinformatics *fastqscreen* *(https://www.bioinformatics.babraham.ac.uk/projects/fastq_screen/)* and *fastQC*

(https://www.bioinformatics.babraham.ac.uk/projects/fastqc/) tools were used to screen the raw reads for containments and to assess quality. We removed traces of the adapter sequence from the raw reads using the *Trimmomatic* tool (Bolger, Lohse et al., 2014). Trimmomatic was also used to trim by quality with the options: *LEADING:3 TRAILING:3 SLIDINGWINDOW:4:15 MINLEN:50*. The trimmed reads were aligned to the mm10 reference genome, using the Burrows-Wheeler Aligner (Li & Durbin, 2010) with the command: > *bwa mem mm10 <pair_1.fq> <pair_2.fq>*. Alignment quality was assessed with the *Qualimap 2.2.1* tool (Okonechnikov, Conesa et al., 2016). The aligned reads were filtered to exclude reads with a MAPQ alignment quality <20. Furthermore, we excluded reads aligning to blacklisted regions identified by the ENCODE consortium (Consortium, 2012). MACS2 version 2.1.1.20160309 was used to identify genomic regions bound by KAP1. We further filtered the aligned reads to retain only those with length 150 and called peaks relative to the input controls using the options ' *--gsize=1.87e9 --qvalue=0.01 -B --keep-dup auto*'. To examine the read density distribution in the vicinity of KAP1 peaks we used *deepTools* (Ramirez, Ryan et al., 2016). Read density was calculated with respect to input using the bamCompare tool from deepTools, with the option '*--binSize 10*'. The matrix of read densities in the vicinity of KAP1 peaks was calculated using '*computeMatrix reference-point*', and heatmaps plotted with '*plotHeatmap*'. The Genomic Association Test tool *GAT* (Heger, Webber et al., 2013) was used to characterise KAP1 binding sites and the relationship between KAP1 and *Paupar*. Coordinates with respect to the mm10 reference genome for characteristic genomic regions (exons, introns, 3' UTRs, etc) were downloaded from the UCSC Genome Table Browser (https://genome.ucsc.edu/cgi-bin/hgTables). The enrichment of KAP1 peaks and the intersection of KAP1 and *Paupar* peaks with respect to these genomic regions was assessed using GAT with the options '--ignore-segment-track –num-samples=100000' and using the complement of the blacklist regions as the workspace. To test for significance coincidence of KAP1 and *Paupar* peaks we use GAT with the same options. The *Paupar* CHART-Seq peakset from (Vance et al., 2014) was used for comparison.

509 **Transcriptomic Analysis**

510 Total RNA was isolated from triplicate control and KAP1 knockdown cells using the Qiagen Mini
511 RNeasy kit following the manufacturer's instructions. RNA samples with a RNA Integrity Number
512 greater than 8, as assessed on a BioAnalyzer (Agilent Technologies), were hybridised to Mouse Gene
513 1.0 ST Arrays as detailed in (Chalei et al., 2014). Differentially expressed genes were identified and
514 Gene Ontology analysis was performed as previously (Vance et al., 2014).

515 **Neurosphere Assay**

516 Neurospheres were cultured according to standard protocols as previously described (Dizon, Shin et
517 al., 2006). In brief, age P3-P6 CD1 pups were anesthetized by hypothermia and decapitated, and the
518 brains were immediately dissected out and sectioned in the coronal plane with a McIlwain tissue
519 chopper. The SVZ was then dissected out in ice-cold HBSS in a sterile laminar flow hood. Accutase
520 was used for 15 mins for dissociation. Cells were cultured in defined Neurobasal media
521 supplemented with 20ng/ml EGF (Sigma) and 20ng/ml bFGF (R&D). Cells were seeded at a density of
522 100 cells/μl and passaged every 3-4 days.

523 **Neural stem cell nucleofection**

524 3-4 x 10^6 dissociated neurosphere cells were nucleofected according to the protocol of LONZA (VPG-
525 1004). Cells were mixed with 100μl nucleofection solution (82μl of Nucleofector Solution + 18μl of
526 supplement) and 5- 10μg DNA and transferred into cuvettes. 500μl of culture medium was added into
527 the cuvette and the sample was then transferred into 1ml medium and centrifuged at 1200rpm for
528 5min and resuspended with fresh medium and plated at 200 000 cells/ 2ml in a polyheme coated 6-
529 well plate.

530 **Postnatal electroporation**

531 Electroporation was performed as published (Boutin, Diestel et al., 2008b, Chesler et al., 2008). DNA
532 plasmids were prepared with Endofree Maxi kit (Qiagen) and mixed with 0.1% fast green for tracing.

DNA concentrations were matched in every individual experiment. P1 CD1 pups were anesthetized with hypothermia and 1-2 µl of plasmids were injected with glass capillary. Electrical pulses (100V, 50ms ON with 850ms intervals for 5 cycles) were given with tweezer electrodes (CUY650P5). Pups were recovered, then returned to dam and analysed at the indicated time.

Immunohistochemistry and imaging

Immunohistochemistry was as previously described (Young, Al-Dalahmah et al., 2014). The following primary antibodies were used: mouse anti-MASH1 (1:100, BD Pharmingen), rabbit anti-KI67 (1:500, Abcam), rabbit anti-CASPASE3 (1:1000, Cell Signaling), rabbit anti-mCherry (1:500, Abcam 167453), rat anti-GFAP (1:500, Invitrogen), chicken anti-GFP (1:500, Aves), rabbit anti-DLX2 (1:50, Abcam). The secondary antibodies were Alexafluor conjugated (Invitrogen). In situ cell death detection kit (Tunel), TMR red (cat# 12156 792910) was used to detect apoptosis. Sections were imaged with Zeiss 710 Laser Scanning Microscopy. For co-localization in GFP+ cells, a 40X oil immersion objective was used and 2µm intervals were used for generating Z-stacks. Confocal images were analysed with ImageJ.

Morphological evaluation

All GFP+ neuroblasts in the granule layer of the OB were binned into Class I, II, or III groups. Only cells with obvious cell bodies and that were entirely found in the field were included. Cells in the rostral migratory stream in the core of the OB, and in OB layers outside of the granule layer were not included. N=3-5 mice per group.

Ethics

All mouse experiments were performed in accordance with institutional and national guidelines and regulations under UK Home Office Project Licence PPL 3003311.

Data availability

Microarray and ChIP-Seq data will be deposited in the GEO database.

ACKNOWLEDGEMENTS

This project has been funded by a Biotechnology and Biological Sciences Research Council grant to KWV (BB/N005856/1; KWV, IP), a Medical Research Council (MR/M010554/1; FGS, BS, FA) grant to FS, and the European Research Council (Project Reference 249869, DARCGENs), the Medical Research Council and Wellcome Trust (CPP, TS).

561 **REFERENCES**

562 Andersen J, Urban N, Achimastou A, Ito A, Simic M, Ullom K, Martynoga B, Lebel M, Goritz C, Frisen J,
563 Nakafuku M, Guillemot F (2014) A transcriptional mechanism integrating inputs from extracellular
564 signals to activate hippocampal stem cells. Neuron 83: 1085-97

565 Bardella C, Al-Dalahmah O, Krell D, Brazauskas P, Al-Qahtani K, Tomkova M, Adam J, Serres S,
566 Lockstone H, Freeman-Mills L, Pfeffer I, Sibson N, Goldin R, Schuster-Boeckler B, Pollard PJ, Soga T,
567 McCullagh JS, Schofield CJ, Mulholland P, Ansorge O et al. (2016) Expression of Idh1R132H in the
568 Murine Subventricular Zone Stem Cell Niche Recapitulates Features of Early Gliomagenesis. Cancer
569 Cell 30: 578-594

570 Bolger AM, Lohse M, Usadel B (2014) Trimmomatic: a flexible trimmer for Illumina sequence data.
571 Bioinformatics 30: 2114-20

572 Boutin C, Diestel S, Desoeuvre A, Tiveron MC, Cremer H (2008a) Efficient in vivo electroporation of the
573 postnatal rodent forebrain. PLoS ONE 3: e1883

574 Boutin C, Diestel S, Desoeuvre A, Tiveron MC, Cremer H (2008b) Efficient In Vivo Electroporation of the
575 Postnatal Rodent Forebrain. Plos One 3

576 Brill MS, Snapyan M, Wohlfrom H, Ninkovic J, Jawerka M, Mastick GS, Ashery-Padan R, Saghatelyan A,
577 Berninger B, Gotz M (2008) A dlx2- and pax6-dependent transcriptional code for periglomerular
578 neuron specification in the adult olfactory bulb. J Neurosci 28: 6439-52

579 Cammas F, Mark M, Dolle P, Dierich A, Chambon P, Losson R (2000) Mice lacking the transcriptional
580 corepressor TIF1beta are defective in early postimplantation development. Development 127: 2955-63

581 Carlson HL, Quinn JJ, Yang YW, Thornburg CK, Chang HY, Stadler HS (2015) LncRNA-HIT Functions as an
582 Epigenetic Regulator of Chondrogenesis through Its Recruitment of p100/CBP Complexes. PLoS
583 genetics 11: e1005680

584 Castro DS, Martynoga B, Parras C, Ramesh V, Pacary E, Johnston C, Drechsel D, Lebel-Potter M, Garcia
585 LG, Hunt C, Dolle D, Bithell A, Ettwiller L, Buckley N, Guillemot F (2011) A novel function of the
586 proneural factor Ascl1 in progenitor proliferation identified by genome-wide characterization of its
587 targets. Genes Dev 25: 930-45

588 Chalei V, Sansom SN, Kong L, Lee S, Montiel JF, Vance KW, Ponting CP (2014) The long non-coding RNA
589 Dali is an epigenetic regulator of neural differentiation. eLife 3: e04530

590 Chang EH, Adorjan I, Mundim MV, Sun B, Dizon ML, Szele FG (2016) Traumatic Brain Injury Activation
591 of the Adult Subventricular Zone Neurogenic Niche. Front Neurosci 10: 332

592 Chesler AT, Le Pichon CE, Brann JH, Araneda RC, Zou DJ, Firestein S (2008) Selective Gene Expression
593 by Postnatal Electroporation during Olfactory Interneuron Nurogenesis. PLoS ONE 3: e1517

594 Chu C, Qu K, Zhong FL, Artandi SE, Chang HY (2011) Genomic maps of long noncoding RNA occupancy
595 reveal principles of RNA-chromatin interactions. Molecular cell 44: 667-78

596 Consortium EP (2012) An integrated encyclopedia of DNA elements in the human genome. Nature
597 489: 57-74

598 Davidovich C, Wang X, Cifuentes-Rojas C, Goodrich KJ, Gooding AR, Lee JT, Cech TR (2015) Toward a
599 consensus on the binding specificity and promiscuity of PRC2 for RNA. Molecular cell 57: 552-8

600 Ding X, Wang X, Lin M, Xing Y, Ge S, Jia R, Zhang H, Fan X, Li J (2016) PAUPAR lncRNA suppresses
601 tumourigenesis by H3K4 demethylation in uveal melanoma. FEBS letters 590: 1729-38

602 Dizon ML, Shin L, Sundholm-Peters NL, Kang E, Szele FG (2006) Subventricular zone cells remain stable
603 in vitro after brain injury. Neuroscience 142: 717-25

604 Doetsch F, Caille I, Lim DA, Garcia-Verdugo JM, Alvarez-Buylla A (1999) Subventricular zone astrocytes
605 are neural stem cells in the adult mammalian brain. Cell 97: 703-16

606 Doetsch F, Garcia-Verdugo JM, Alvarez-Buylla A (1997) Cellular composition and three-dimensional
607 organization of the subventricular germinal zone in the adult mammalian brain. J Neurosci 17: 5046-61

608 Engreitz JM, Haines JE, Perez EM, Munson G, Chen J, Kane M, McDonel PE, Guttman M, Lander ES
609 (2016) Local regulation of gene expression by lncRNA promoters, transcription and splicing. Nature
610 539: 452-455

611 Heger A, Webber C, Goodson M, Ponting CP, Lunter G (2013) GAT: a simulation framework for testing
612 the association of genomic intervals. Bioinformatics 29: 2046-8

613 Herzog M, Wendling O, Guillou F, Chambon P, Mark M, Losson R, Cammas F (2011) TIF1beta
614 association with HP1 is essential for post-gastrulation development, but not for Sertoli cell functions
615 during spermatogenesis. Developmental biology 350: 548-58

616 Hsieh MJ, Yao YL, Lai IL, Yang WM (2006) Transcriptional repression activity of PAX3 is modulated by
617 competition between corepressor KAP1 and heterochromatin protein 1. Biochemical and biophysical
618 research communications 349: 573-81

619 Ilik IA, Quinn JJ, Georgiev P, Tavares-Cadete F, Maticzka D, Toscano S, Wan Y, Spitale RC, Luscombe N,
620 Backofen R, Chang HY, Akhtar A (2013) Tandem stem-loops in roX RNAs act together to mediate X
621 chromosome dosage compensation in Drosophila. Molecular cell 51: 156-73

622 Iyengar S, Farnham PJ (2011) KAP1 protein: an enigmatic master regulator of the genome. The Journal
623 of biological chemistry 286: 26267-76

624 Iyengar S, Ivanov AV, Jin VX, Rauscher FJ, 3rd, Farnham PJ (2011) Functional analysis of KAP1 genomic
625 recruitment. Molecular and cellular biology 31: 1833-47

626 Kaneko S, Son J, Shen SS, Reinberg D, Bonasio R (2013) PRC2 binds active promoters and contacts
627 nascent RNAs in embryonic stem cells. Nat Struct Mol Biol 20: 1258-64

628 Li H, Durbin R (2010) Fast and accurate long-read alignment with Burrows-Wheeler transform.
629 Bioinformatics 26: 589-95

630 Maenner S, Muller M, Frohlich J, Langer D, Becker PB (2013) ATP-dependent roX RNA remodeling by
631 the helicase maleless enables specific association of MSL proteins. Molecular cell 51: 174-84

632 Mercer TR, Dinger ME, Sunkin SM, Mehler MF, Mattick JS (2008) Specific expression of long noncoding
633 RNAs in the mouse brain. Proceedings of the National Academy of Sciences of the United States of
634 America 105: 716-21

635 Mercer TR, Qureshi IA, Gokhan S, Dinger ME, Li G, Mattick JS, Mehler MF (2010) Long noncoding RNAs
636 in neuronal-glial fate specification and oligodendrocyte lineage maturation. BMC neuroscience 11: 14

637 Nowak DE, Tian B, Brasier AR (2005) Two-step cross-linking method for identification of NF-kappaB
638 gene network by chromatin immunoprecipitation. Biotechniques 39: 715-25

639 O'Geen H, Squazzo SL, Iyengar S, Blahnik K, Rinn JL, Chang HY, Green R, Farnham PJ (2007) Genome-
640 wide analysis of KAP1 binding suggests autoregulation of KRAB-ZNFs. PLoS genetics 3: e89

641 Okonechnikov K, Conesa A, Garcia-Alcalde F (2016) Qualimap 2: advanced multi-sample quality control
642 for high-throughput sequencing data. Bioinformatics 32: 292-4

643 Ponjavic J, Oliver PL, Lunter G, Ponting CP (2009) Genomic and transcriptional co-localization of
644 protein-coding and long non-coding RNA pairs in the developing brain. PLoS genetics 5: e1000617

645 Portoso M, Ragazzini R, Brencic Z, Moiani A, Michaud A, Vassilev I, Wassef M, Servant N, Sargueil B,
646 Margueron R (2017) PRC2 is dispensable for HOTAIR-mediated transcriptional repression. The EMBO
647 journal 36: 981-994

648 Pradeepa MM, McKenna F, Taylor GC, Bengani H, Grimes GR, Wood AJ, Bhatia S, Bickmore WA (2017)
649 Psip1/p52 regulates posterior Hoxa genes through activation of lncRNA Hottip. PLoS genetics 13:
650 e1006677

651 Ramirez F, Ryan DP, Gruning B, Bhardwaj V, Kilpert F, Richter AS, Heyne S, Dundar F, Manke T (2016)
652 deepTools2: a next generation web server for deep-sequencing data analysis. Nucleic Acids Res 44:
653 W160-5

654 Ramos AD, Diaz A, Nellore A, Delgado RN, Park KY, Gonzales-Roybal G, Oldham MC, Song JS, Lim DA
655 (2013) Integration of genome-wide approaches identifies lncRNAs of adult neural stem cells and their
656 progeny in vivo. Cell stem cell 12: 616-28

657 Rutenberg-Schoenberg M, Sexton AN, Simon MD (2016) The Properties of Long Noncoding RNAs That
658 Regulate Chromatin. Annu Rev Genomics Hum Genet 17: 69-94

659 Schultz DC, Ayyanathan K, Negorev D, Maul GG, Rauscher FJ, 3rd (2002) SETDB1: a novel KAP-1-
660 associated histone H3, lysine 9-specific methyltransferase that contributes to HP1-mediated silencing
661 of euchromatic genes by KRAB zinc-finger proteins. Genes & development 16: 919-32

662 Shibata M, Blauvelt KE, Liem KF, Jr., Garcia-Garcia MJ (2011) TRIM28 is required by the mouse KRAB
663 domain protein ZFP568 to control convergent extension and morphogenesis of extra-embryonic
664 tissues. Development 138: 5333-43

665 Suh Y, Obernier K, Holzl-Wenig G, Mandl C, Herrmann A, Worner K, Eckstein V, Ciccolini F (2009)
666 Interaction between DLX2 and EGFR regulates proliferation and neurogenesis of SVZ precursors. Mol
667 Cell Neurosci 42: 308-14

668 Tsai MC, Manor O, Wan Y, Mosammaparast N, Wang JK, Lan F, Shi Y, Segal E, Chang HY (2010) Long
669 noncoding RNA as modular scaffold of histone modification complexes. Science 329: 689-93

670 Vance KW (2016) Mapping long non-coding RNA chromatin occupancy using Capture Hybridization
671 Analysis of RNA Targets (CHART). Methods In Molecular Biology

672 Vance KW, Ponting CP (2014) Transcriptional regulatory functions of nuclear long noncoding RNAs.
673 Trends in genetics : TIG 30: 348-55

674 Vance KW, Sansom SN, Lee S, Chalei V, Kong L, Cooper SE, Oliver PL, Ponting CP (2014) The long non-
675 coding RNA Paupar regulates the expression of both local and distal genes. The EMBO journal 33: 296-
676 311

677 West JA, Davis CP, Sunwoo H, Simon MD, Sadreyev RI, Wang PI, Tolstorukov MY, Kingston RE (2014)
678 The long noncoding RNAs NEAT1 and MALAT1 bind active chromatin sites. Molecular cell 55: 791-802

679 Yang HK, Sundholm-Peters NL, Goings GE, Walker AS, Hyland K, Szele FG (2004) Distribution of
680 doublecortin expressing cells near the lateral ventricles in the adult mouse brain. J Neurosci Res 76:
681 282-95

682 Yang L, Lin C, Jin C, Yang JC, Tanasa B, Li W, Merkurjev D, Ohgi KA, Meng D, Zhang J, Evans CP,
683 Rosenfeld MG (2013) lncRNA-dependent mechanisms of androgen-receptor-regulated gene activation
684 programs. Nature 500: 598-602

685 Yang YW, Flynn RA, Chen Y, Qu K, Wan B, Wang KC, Lei M, Chang HY (2014) Essential role of lncRNA
686 binding for WDR5 maintenance of active chromatin and embryonic stem cell pluripotency. eLife 3:
687 e02046

688 Yin Y, Yan P, Lu J, Song G, Zhu Y, Li Z, Zhao Y, Shen B, Huang X, Zhu H, Orkin SH, Shen X (2015) Opposing
689 Roles for the lncRNA Haunt and Its Genomic Locus in Regulating HOXA Gene Activation during
690 Embryonic Stem Cell Differentiation. Cell stem cell 16: 504-16

691 Young CC, Al-Dalahmah O, Lewis NJ, Brooks KJ, Jenkins MM, Poirier F, Buchan AM, Szele FG (2014)
692 Blocked angiogenesis in Galectin-3 null mice does not alter cellular and behavioral recovery after
693 middle cerebral artery occlusion stroke. Neurobiol Dis 63: 155-64

694 Zhao J, Ohsumi TK, Kung JT, Ogawa Y, Grau DJ, Sarma K, Song JJ, Kingston RE, Borowsky M, Lee JT
695 (2010) Genome-wide identification of polycomb-associated RNAs by RIP-seq. Molecular cell 40: 939-53

696

697

FIGURE LEGENDS

Figure 1. *Paupar* directly binds the KAP1 chromatin regulatory protein in mouse N2A neuroblastoma cells. (a) Overview of the pull down assay. *In vitro* transcribed biotinylated *Paupar* RNA was immobilised on streptavidin beads and incubated with N2A cell nuclear extract. Bound RNA protein complexes were extensively washed and specific *Paupar* associated proteins, which do not interact with a control mRNA of a similar size, identified by mass spectrometry. (b) Gene Ontology terms were used to annotate *Paupar* associated proteins according to biological process. The Bonferroni correction was used to adjust the P-values to correct for multiple testing. (c) Endogenous *Paupar* transcript interacts with transcription and chromatin regulatory proteins in N2A cells. *Paupar* association with the indicated proteins was measured using native RNA-IP. Whole cell lysates were prepared and the indicated regulatory proteins immuno-precipitated using specific antibodies. Bound RNAs were purified and the levels of *Paupar* and the *U1snRNA* control detected in each RIP using qRT-PCR. *Paupar* transcript directly interacts with KAP1 and RCOR3 in N2A cells. Nuclear extracts were prepared from UV cross-linked (d) and untreated (e) cells and immuno-precipitated using either anti-KAP1, anti-RCOR3 or a rabbit IgG control antibody. Associated RNAs were stringently washed and purified. The levels of *Paupar* and a *U1snRNA* control transcript were detected in each UV-RIP using qRT-PCR. Results are presented as fold enrichment relative to control antibody. Mean values +/- SEM., N=3. One-tailed t-test, unequal variance *p<0.05, **p<0.01, ***p<0.001 (f) PAX6 associates with KAP1 in N2A cells. FLAG-PAX6 and KAP1 or RCOR3 expression vectors were transfected into N2A cells. Lysates were prepared two days after transfection and FLAG-PAX6 protein immuno-precipitated using anti-FLAG beads. Co-precipitated proteins were detected by western blotting.

Figure 2. *Paupar* and KAP1 regulate shared target genes involved in neural cell proliferation and function. N2A cells were transfected with either the shA *Kap1* targeting shRNA expression vector or a scrambled control and pTK-Hyg selection plasmid. Three days later cells were expanded and

723 hygromycin was added to the medium to remove untransfected cells. (a) After seven days, western
724 blotting was performed to determine KAP1 protein levels. LAMINB1 was used as a loading control.
725 (b) *Kap1* and *Paupar* transcript levels were analysed by qRT-PCR. Data was normalised using *Gapdh*
726 and expression changes are shown relative to a non-targeting scrambled control (set at 1). Mean
727 values +/- SEM., N=3. One-tailed t-test, unequal variance **p<0.01 (c) KAP1 regulated genes were
728 identified using a GeneChip Mouse Gene 1.0 ST Array (5% FDR, log2 fold change > 0.5). (d)
729 Intersection of *Kap1* and *Paupar* regulated genes revealed common target genes whose expression is
730 controlled by both these factors. (e) The majority (87%) of *Paupar* and *Kap1* shared target genes are
731 positively regulated by *Paupar.* (f) Gene Ontology analysis of *Paupar* and *Kap1* common target genes
732 was performed using GOToolBox. Representative significantly enriched categories were selected
733 from a hypergeometric test with a Benjamini-Hochberg corrected P-value threshold of 0.05.

734 **Figure 3. *Paupar* promotes KAP1 chromatin occupancy and H3K9me3 deposition at PAX6 bound**
735 **sequences within the regulatory regions of common targets.** (a) Intersection of *Paupar*, KAP1 and
736 PAX6 regulated genes identified 87 common target genes. 34 of these genes (in brackets) contain a
737 *Paupar* binding site within their regulatory regions. (b) ChIP assays were performed in N2A cells using
738 either an antibody against KAP1 or an isotype specific control. (c) N2A cells were transfected with
739 either a non-targeting control or two independent *Paupar* targeting shRNA expression vectors. Cells
740 were harvested for ChIP three days later. *Paupar* depletion was confirmed using qRT-PCR. (d) *Paupar*
741 knockdown reduces KAP1 chromatin occupancy at shared binding sites. ChIP assays were performed
742 using either an anti-KAP1 polyclonal antibody or a normal IgG rabbit control. (e) Western blotting
743 showed that KAP1 proteins levels do not change upon *Paupar* knockdown. ACTIN was used as a
744 control. (f) *Paupar* promotes PAX6-KAP1 association. FLAG-PAX6 and KAP1 expression vectors were
745 co-transfected into N2A cells along with increasing concentrations of *Paupar* or a size matched
746 control lncRNA expression vector. Expression of the maximum concentration of either *Paupar* or
747 control RNA in each IP does not alter KAP1 input protein levels (lower panel). Lysates were prepared
748 two days after transfection and FLAG-PAX6 protein immuno-precipitated using anti-FLAG beads. The

749 amount of DNA transfected was made equal in each IP using empty vector and proteins in each
750 complex were detected by western blotting. (g, h) *Paupar* knockdown reduces H3K9me3 at a subset
751 of bound sequences in *trans*. For ChIP assays, the indicated DNA fragments were amplified using
752 qPCR. % input was calculated as 100*2^(Ct Input-Ct IP). Results are presented as mean values +/-
753 SEM, N=3. One-tailed t-test, unequal variance *p<0.05, **p<0.01, ***p<0.001

754 **Figure 4. *Paupar* co-occupies a subset of KAP1 binding sites on chromatin genome-wide.** 5510 KAP1
755 binding sites common to both replicates were identified relative to input DNA (1% FDR)
756 (Supplemental Table S4). (a) GAT analysis shows that the sites of KAP1 occupancy are particularly
757 enriched at promoter regions (5'UTRs), over gene bodies and over the 3'UTR exons of zinc finger
758 genes (q = 0.00002). (b) Intersection of KAP1 and *Paupar* binding sites in N2A cells identified 46 KAP1
759 bound locations that are specifically co-occupied by *Paupar.* This represents a significant (p < 0.001)
760 4-fold enrichment as estimated using GAT. (c) Sequencing read density distribution over the 46
761 shared binding locations was calculated and revealed a coincidence of *Paupar* and KAP1 binding site
762 centrality.

763 **Figure 5. *Paupar* and Kap1 regulate SVZ neurogenesis *in vivo*.** P1 pups were electroporated with the
764 indicated shRNA expression vectors. All shRNA plasmids also express GFP. (a) Example of co-
765 immunostaining of MASH1, KI67 and GFP in the SVZ with electroporated GFP+ cells. White arrows in
766 top row indicate MASH1+/GFP+ cells 24hpe. Magenta arrows in bottom row (different field) indicate
767 KI67+/GFP+ cells. (b) Quantification after *Paupar* knockdown of the percent of GFP+ cells in the SVZ
768 that express GFAP, MASH1, DLX2 or KI67 at 24hpe. N≥3. (c) Immunostaining of GFP and GFAP in the
769 SVZ, 3dpe. The small arrows indicate GFAP+/GFP+ cells. (d-e) Quantification after *Paupar* knockdown
770 of the percent of GFP+ cells that express GFAP, MASH1 or KI67 at 3dpe. N≥4. (f) Example of co-
771 immunostaining of GFP and MASH1 in the SVZ, 3dpe. The small arrows indicate MASH1+/GFP+ cells.
772 (g) Quantification after *Kap1* knockdown of the percent of GFP+ cells that express GFAP, MASH1,

DLX2 or KI67 at 3 dpe. N=3. Data are shown as mean ± SEM and analysed by two-tailed Student t-tests. *p<0.05, **p<0.01, ***p<0.001. Scale bars represent 20 μm (a), 50 μm (c).

Figure 6. *Paupar* and *Kap1* loss of function alters OB neuron morphology. P1 pups were electroporated with the indicated shRNA expression vectors. All shRNA plasmids also express GFP. (a, b) Immunostaining and quantification of GFP+ cells that were electroporated in the SVZ and migrated to the OB, *Paupar* KD, 7dpe. N≥3. (c-d) GFP+ cells that have migrated to the olfactory bulb 7dpe decrease after *Kap1* KD. Quantification of the density of electroporated cells in the OB after *Kap1* KD. N=3. (e) High magnification showing different morphologies in GFP+ granule layer OB neurons 7 dpe, *Paupar* KD. For ease of comparison neuronal orientations were aligned to vertical. The cells shown in the scr control group are class I N≥3. (f) High magnification showing different morphologies in GFP+ granule layer OB neurons 7 dpe, *Kap1* KD. Neuronal orientations rendered vertical. The scr control image shows several class I as well as class III neurons. (N=3). (g) Quantification of the percent of cells with Class I and Class III morphology 7 days after *Paupar* KD. (h) Quantification of the percent of cells with Class I and Class III morphology 7 days after *Kap1* KD. Data are shown as mean ± SEM and analysed by two-tailed Student t-tests. *p<0.05, **p<0.01, ***p<0.001. Scale bars represent 100 μm (a), 200 μm (c), 30 μm (e), 50 μm (f).

Figure 7. Schematic detailing possible *Paupar* mode of action at distal bound regulatory regions. *Paupar* promotes KAP1 chromatin association and H3K9me3 deposition through the assembly of a DNA bound ribonucleoprotein complex containing *Paupar*, KAP1 and PAX6 within the regulatory regions of the *Mab21L2*, *Mst1*, *E2f2* and *Igfbp5* direct target genes. We propose three potential (non-mutually exclusive) scenarios to describe the order of assembly of this complex: (i) A ternary complex forms in the nucleoplasm before binding DNA; (ii) *Paupar* interacts with KAP1 and guides it to DNA bound PAX6; or (iii) KAP1 is recruited to a DNA bound PAX6-*Paupar* complex. This leads to local H3K9me3 modification changes at these bound sequences in *trans*. The model was generated taking into consideration the discovery that *Paupar* genome wide binding sites contain an enrichment of

798 motifs for neural transcription factors but are not enriched for sequences that are complementary to
799 *Paupar* itself (Vance et al., 2014). This suggests that *Paupar* does not bind DNA directly but is
800 targeted to chromatin indirectly through RNA-protein interactions with transcription factors such as
801 PAX6. Moreover, KAP1 is a non-DNA binding chromatin regulator that is also targeted to the genome
802 through interactions with transcription factors.

803 **SUPPLEMENTAL MATERIAL**

804 **Supplemental Tables**

805 Supplemental Table S1: Specific *Paupar* Associated Proteins

806 Supplemental Table S2: KAP1 Regulated Genes

807 Supplemental Table S3: Shared Target Genes

808 Supplemental Table S4: KAP1 ChIP-seq binding locations

809 Supplemental Table S5: Oligos

810 **Supplemental Figure Legends**

811 **Supplemental Figure S1.** (a) Nuclear extracts were prepared from UV cross-linked N2A cells and
812 immuno-precipitated using either the indicated antibodies or a rabbit IgG control antibody.
813 Associated RNAs were stringently washed and purified. The levels of *Paupar* and *U1snRNA* were
814 detected in each UV-RIP using qRT-PCR. Results are presented as fold enrichment relative to control
815 antibody. Mean values +/- SEM. (b) N2A cells were transfected with an additional Kap1 targeting
816 shRNA expression vector shB-Kap1 or a scrambled control plasmid. Three days later cells were
817 harvested and expression analysed using RT-qPCR. Samples were normalised using *Gapdh* and the
818 results are presented relative to the control. Results are presented as mean values +/- SEM, N=3; *P
819 < 0.05, one-tailed t-test, unequal variance.

820 **Supplemental Figure S2.** *Paupar*-KAP1-PAX6 bound sequences within the regulatory regions of the
821 *Mab21L2*, *Mst1*, *E2f2, Igfbp5* and *Ezh2* genes are enriched in H3K9me3 modified chromatin. ChIP
822 assays were performed in N2A cells using either histone H3K9me3 or anti-rabbit IgG control
823 antibody. DNA fragments were amplified using qPCR. % input was calculated as 100*2^(Ct Input-Ct
824 IP). Results are presented as mean values +/- SEM., N=4.

825

826 **Supplemental Figure S3. *Paupar* knockdown in SVZ.** (a) *Paupar* transcript detected using RT-qPCR in
827 the P4 SVZ and in tertiary neurospheres prepared from the P4 SVZ. (b) *Paupar* knockdown in tertiary
828 neurospheres with sh165 and sh408. Neurosphere cultures were transfected with the indicated
829 *Paupar* targeting shRNA expression vectors or a non-targeting control. *Paupar* expression was
830 quantified using qRT-PCR three days later and normalised using *Gapdh*. The results are presented
831 relative to the scrambled control (set at 1). (N≥4). (c) Immunostaining of GFP and mCherry in SVZ
832 electroporated with shRNA and pCS-tdTomato at 24hpe. The concentration of the constructs were
833 matched in order to minimize electroporation efficiency differences between scramble, sh165 and
834 sh408. Fewer GFP+ cells were found in the SVZ after sh165 electroporation compared to scramble
835 control electroporation. Co-electroporation with a construct expressing tdTomato driven by a different
836 promoter (pCS), confirmed this was not due to the sh165 construct itself as fewer tdTomato+ cells
837 were also observed at 24hpe. Knockdown with sh408 resulted in similar numbers of GFP+
838 electroporated cells compared to scramble controls at 24hpe. N=3. (d) GFP and DCX co-labelling in the
839 OB 7dpe. Small red arrows show examples of co-labelled cells. There are no error bars because 100%
840 of all GFP+ cells in the OB were DCX+. Data are shown as mean ± SEM and analysed by two-tailed
841 Student t-tests. *p<0.05, **p<0.01, ***p<0.001. Scale bars represent 150 μm (c), and 30 μm (d).

842 **Supplemental Figure S4. Cell death analysis after *Paupar* and Kap1 KD.** (a) Immunostaining of GFP
843 and CASPASE3 in SVZ at 3dpe. N=4. (b-c) Tunel assay and quantification in the SVZ after *Paupar* KD
844 3dpe. N=3. (d-e) Tunel assay and quantification in the SVZ after Kap1 KD 3dpe. N=3. Data are shown as
845 mean ± SEM and analysed by one-way ANOVA. Data are shown as mean ± SEM and analysed by two-
846 tailed Student t-tests. Scale bars represent 50 μm (a), 30 μm (b,d).

847

Figure 1

a

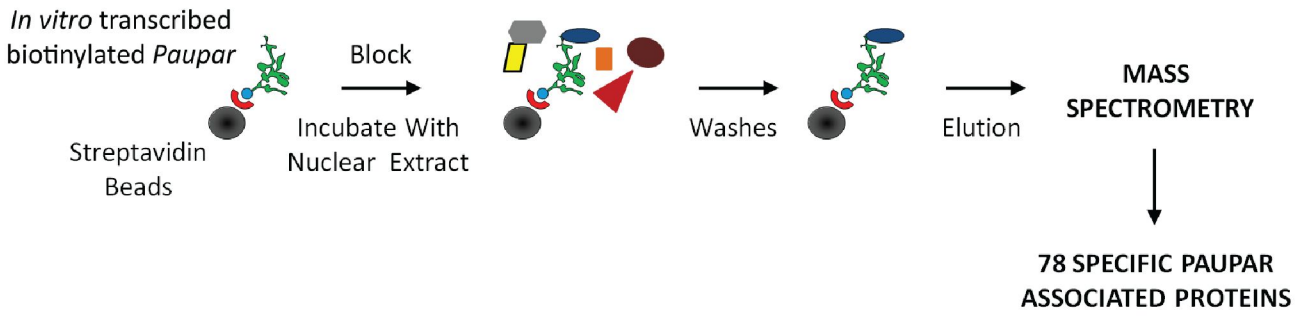

b

GOID	Term	Number In Set	Number In Reference	Corrected P-value
GO:0006396	RNA processing	19	513	3.35×10^{-12}
GO:0008380	RNA splicing	13	237	6.72×10^{-10}
GO:0022613	ribonucleoprotein complex biogenesis	10	195	5.87×10^{-7}
GO:0010467	gene expression	28	3596	5.44×10^{-3}

c

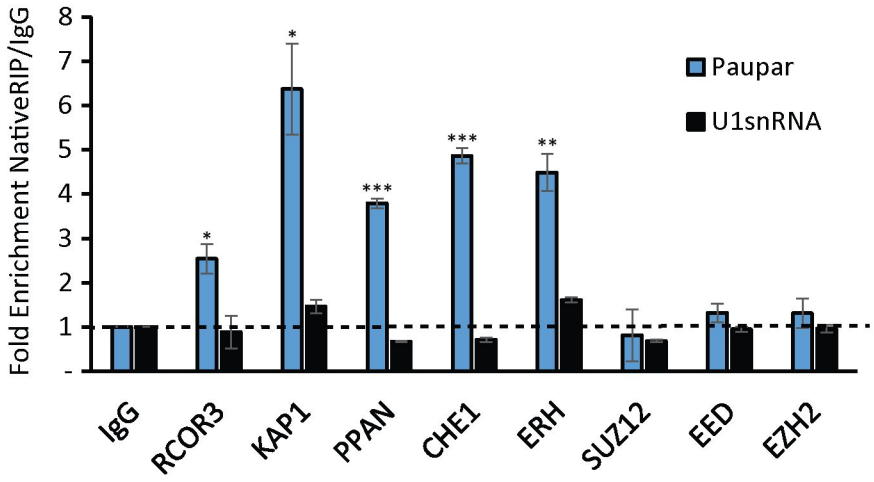

d

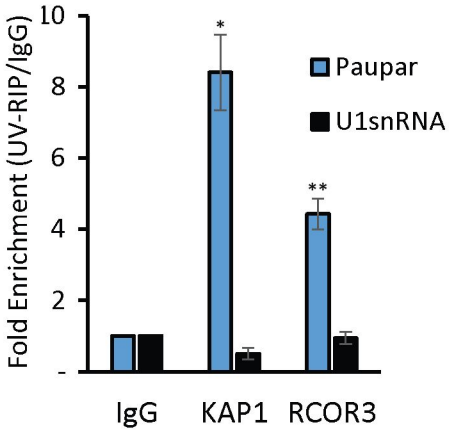

e

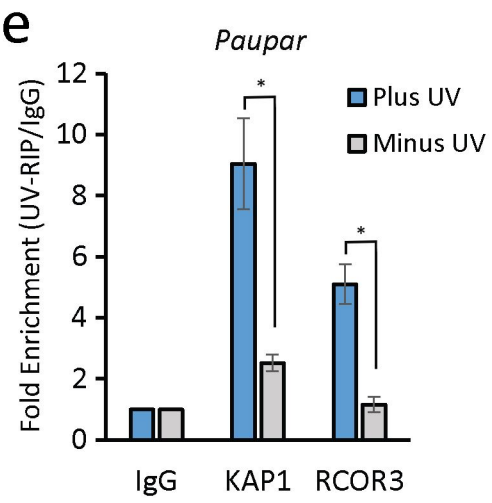

f

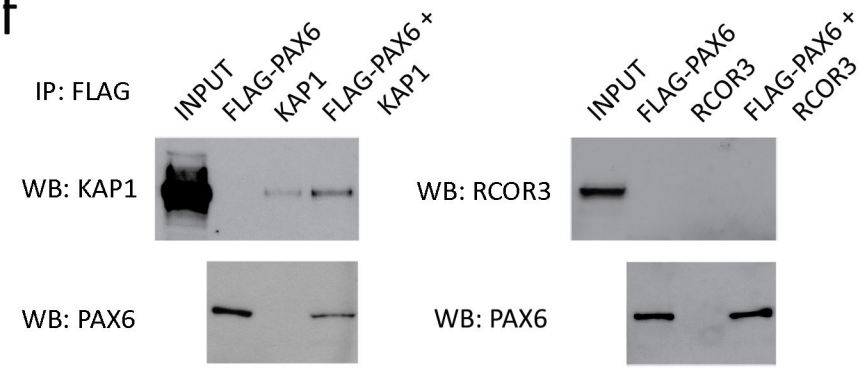

Figure 2

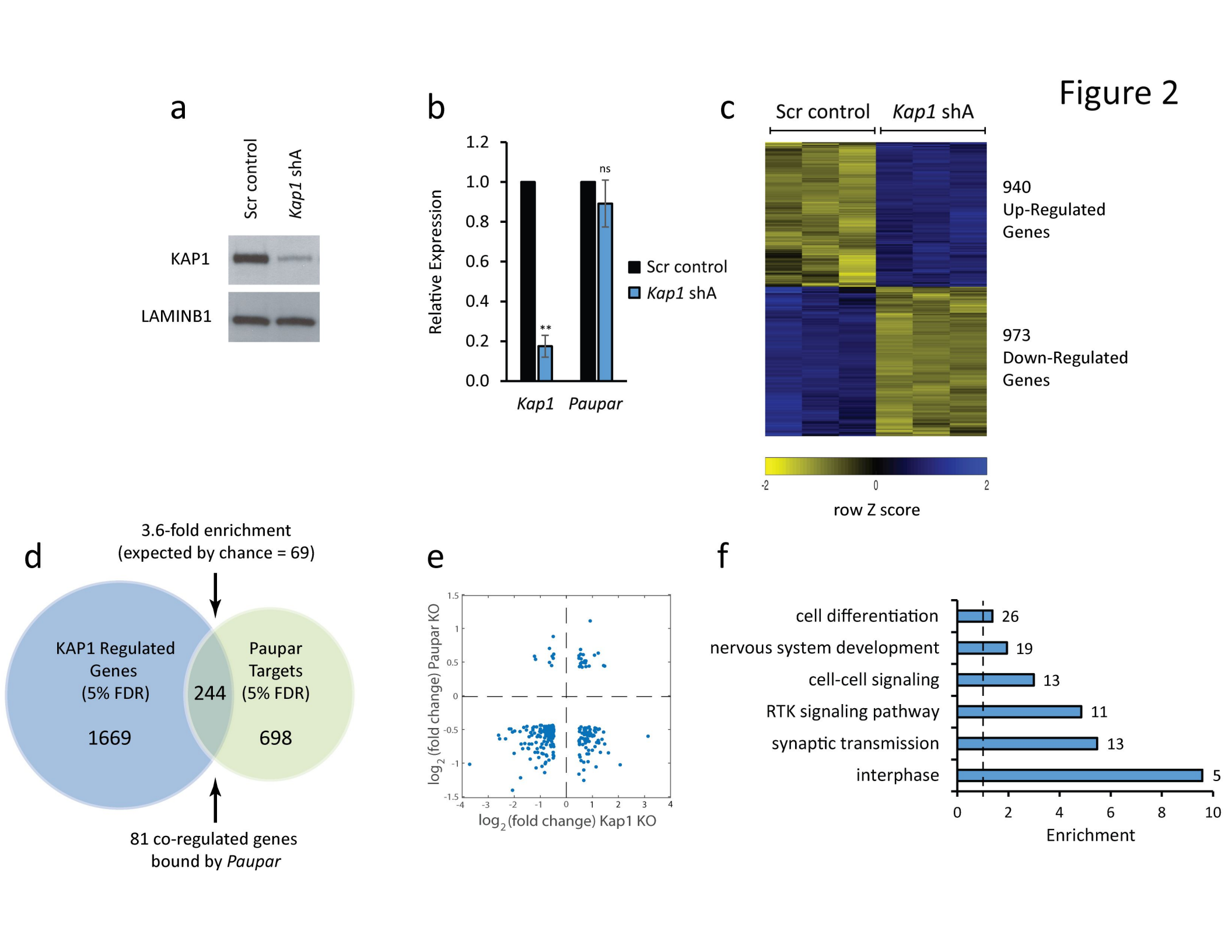
a
Scr control
Kap1 shA
KAP1
LAMINB1
b
Relative Expression
1.2
1.0
0.8
0.6
0.4
0.2
0.0
**
ns
Scr control
Kap1 shA
Kap1
Paupar
c
Scr control
Kap1 shA
940
Up-Regulated
Genes
973
Down-Regulated
Genes
-2
0
2
row Z score
d
3.6-fold enrichment
(expected by chance = 69)
KAP1 Regulated
Genes
(5% FDR)
1669
244
Paupar
Targets
(5% FDR)
698
81 co-regulated genes
bound by Paupar
e
log2 (fold change) Paupar KO
log2 (fold change) Kap1 KO
f
cell differentiation
26
nervous system development
19
cell-cell signaling
13
RTK signaling pathway
11
synaptic transmission
13
interphase
5
0
2
4
6
8
10
Enrichment

Figure 3

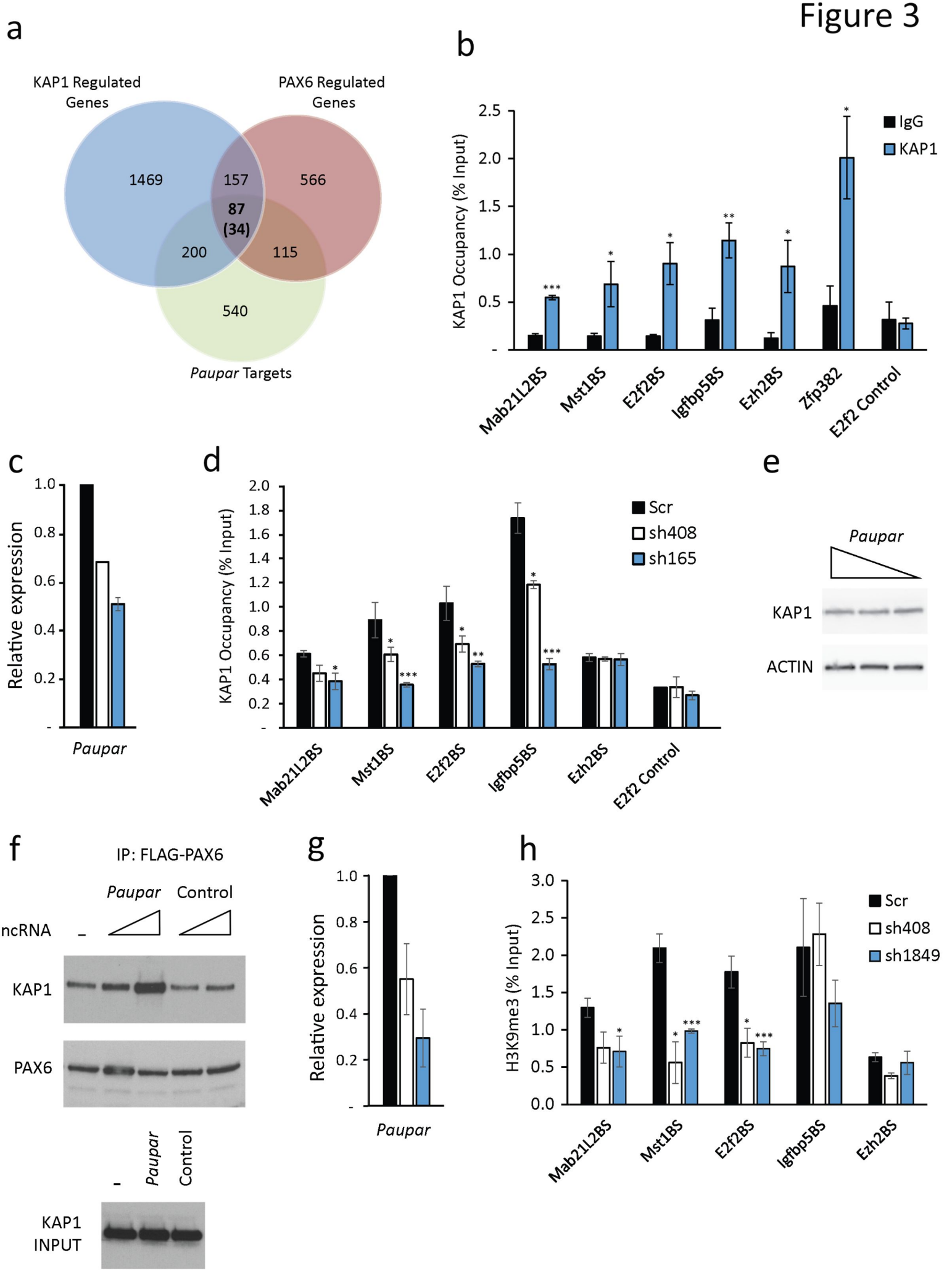
a
KAP1 Regulated Genes
PAX6 Regulated Genes
1469
157
566
87 (34)
200
115
540
Paupar Targets
b
KAP1 Occupancy (% Input)
IgG
KAP1
Mab21L2BS
Mst1BS
E2f2BS
Igfbp5BS
Ezh2BS
Zfp382
E2f2 Control
c
Relative expression
Paupar
d
KAP1 Occupancy (% Input)
Scr
sh408
sh165
Mab21L2BS
Mst1BS
E2f2BS
Igfbp5BS
Ezh2BS
E2f2 Control
e
Paupar
KAP1
ACTIN
f
IP: FLAG-PAX6
Paupar
Control
lncRNA
KAP1
PAX6
Paupar
Control
KAP1
INPUT
g
Relative expression
Paupar
h
H3K9me3 (% Input)
Scr
sh408
sh1849
Mab21L2BS
Mst1BS
E2f2BS
Igfbp5BS
Ezh2BS

Figure 4

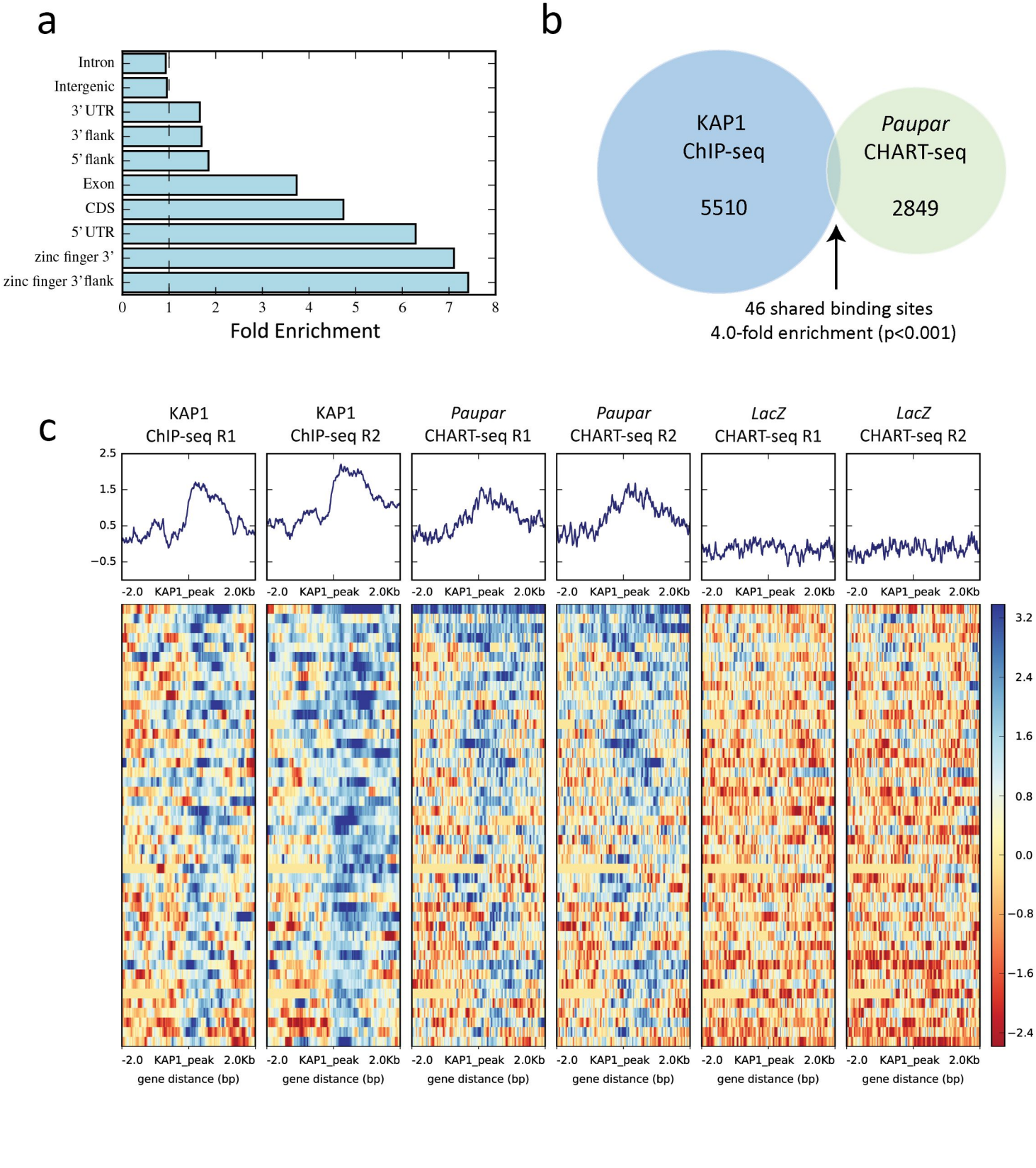
a
Intron
Intergenic
3' UTR
3' flank
5' flank
Exon
CDS
5' UTR
zinc finger 3'
zinc finger 3' flank
0
1
2
3
4
5
6
7
8
Fold Enrichment
b
KAP1
ChIP-seq
5510
Paupar
CHART-seq
2849
46 shared binding sites
4.0-fold enrichment (p<0.001)
c
KAP1
ChIP-seq R1
KAP1
ChIP-seq R2
Paupar
CHART-seq R1
Paupar
CHART-seq R2
LacZ
CHART-seq R1
LacZ
CHART-seq R2
2.5
1.5
0.5
−0.5
-2.0 KAP1_peak 2.0Kb
gene distance (bp)
3.2
2.4
1.6
0.8
0.0
−0.8
−1.6
−2.4

Figure 5

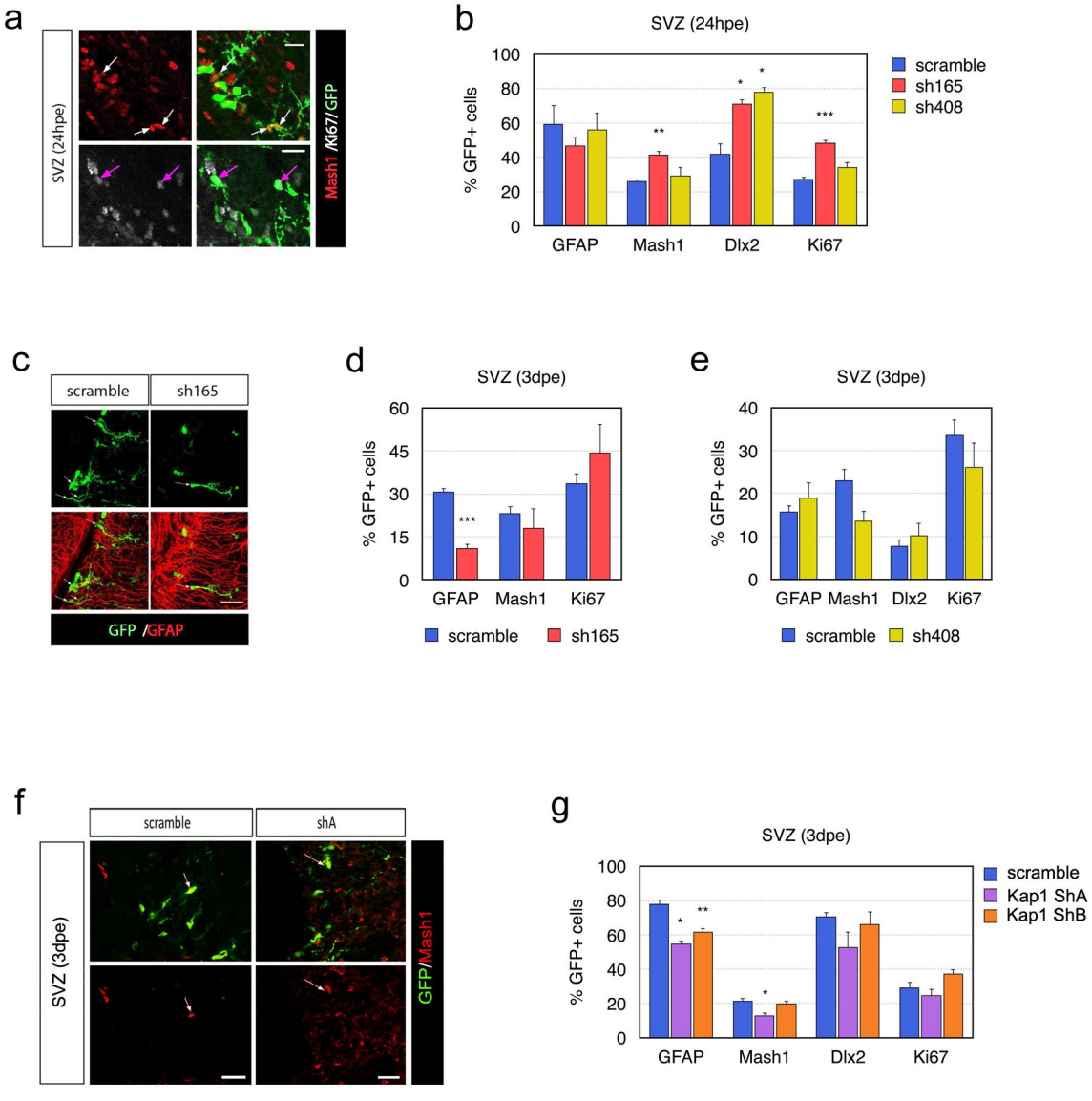
a
SVZ (24hpe)
Mash1 /Ki67/ GFP
b
SVZ (24hpe)
% GFP+ cells
100
80
60
40
20
0
GFAP
Mash1
Dlx2
Ki67
scramble
sh165
sh408
c
scramble
sh165
GFP /GFAP
d
SVZ (3dpe)
% GFP+ cells
60
45
30
15
0
GFAP
Mash1
Ki67
scramble
sh165
e
SVZ (3dpe)
% GFP+ cells
40
30
20
10
0
GFAP
Mash1
Dlx2
Ki67
scramble
sh408
f
scramble
shA
SVZ (3dpe)
GFP/Mash1
g
SVZ (3dpe)
% GFP+ cells
100
80
60
40
20
0
GFAP
Mash1
Dlx2
Ki67
scramble
Kap1 ShA
Kap1 ShB

Figure 6

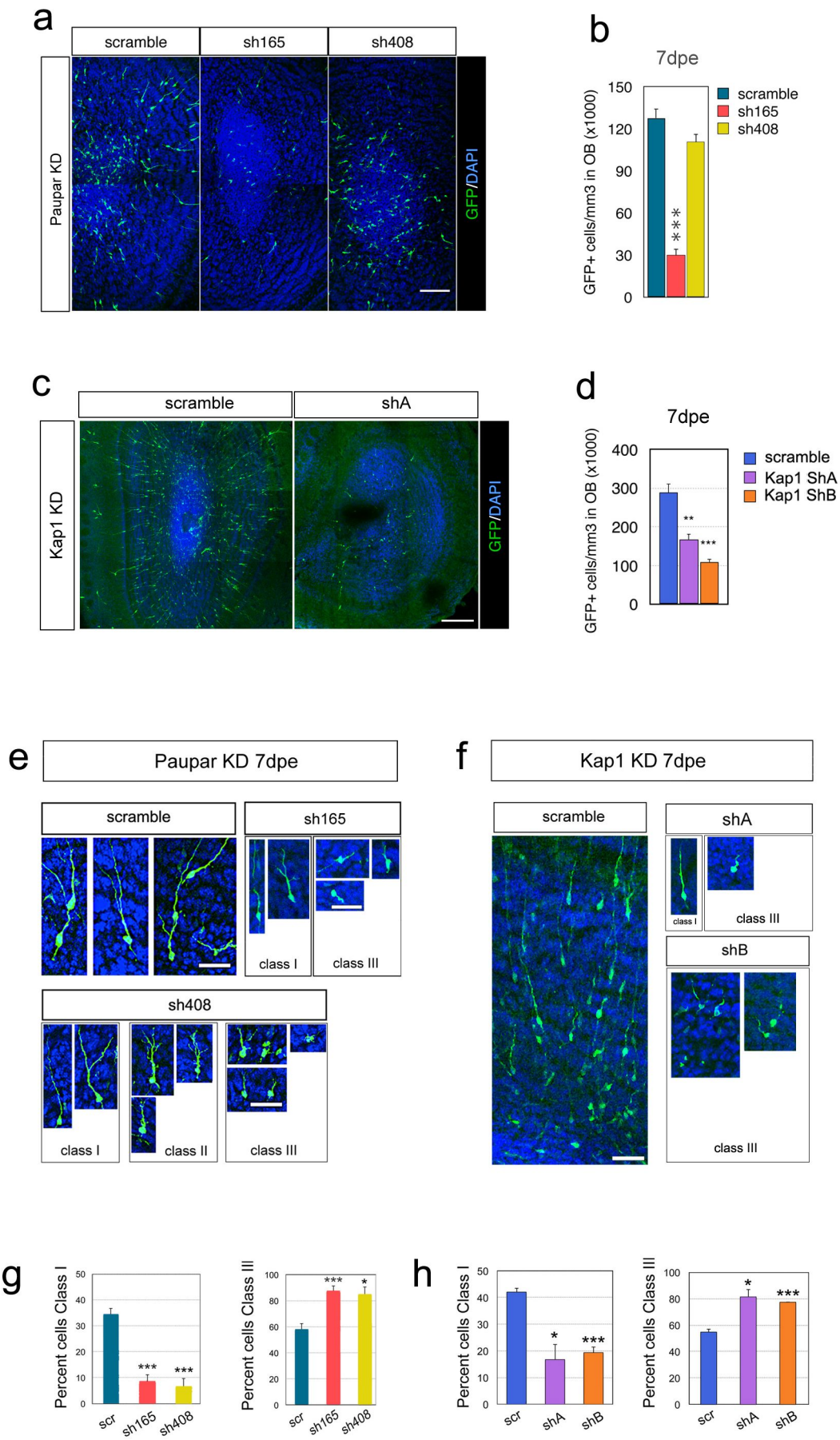
a
scramble
sh165
sh408
Paupar KD
GFP/DAPI
b
7dpe
GFP+ cells/mm3 in OB (x1000)
150
120
90
60
30
0
***
scramble
sh165
sh408
c
scramble
shA
Kap1 KD
GFP/DAPI
d
7dpe
GFP+ cells/mm3 in OB (x1000)
400
300
200
100
0
**
***
scramble
Kap1 ShA
Kap1 ShB
e
Paupar KD 7dpe
scramble
sh165
class I
class III
sh408
class I
class II
class III
f
Kap1 KD 7dpe
scramble
shA
class I
class III
shB
class III
g
Percent cells Class I
50
40
30
20
10
0
***
***
scr
sh165
sh408
Percent cells Class III
100
80
60
40
20
0
***
*
scr
sh165
sh408
h
Percent cells Class I
50
40
30
20
10
0
*
***
scr
shA
shB
Percent cells Class III
100
80
60
40
20
0
*
***
scr
shA
shB

Figure 7

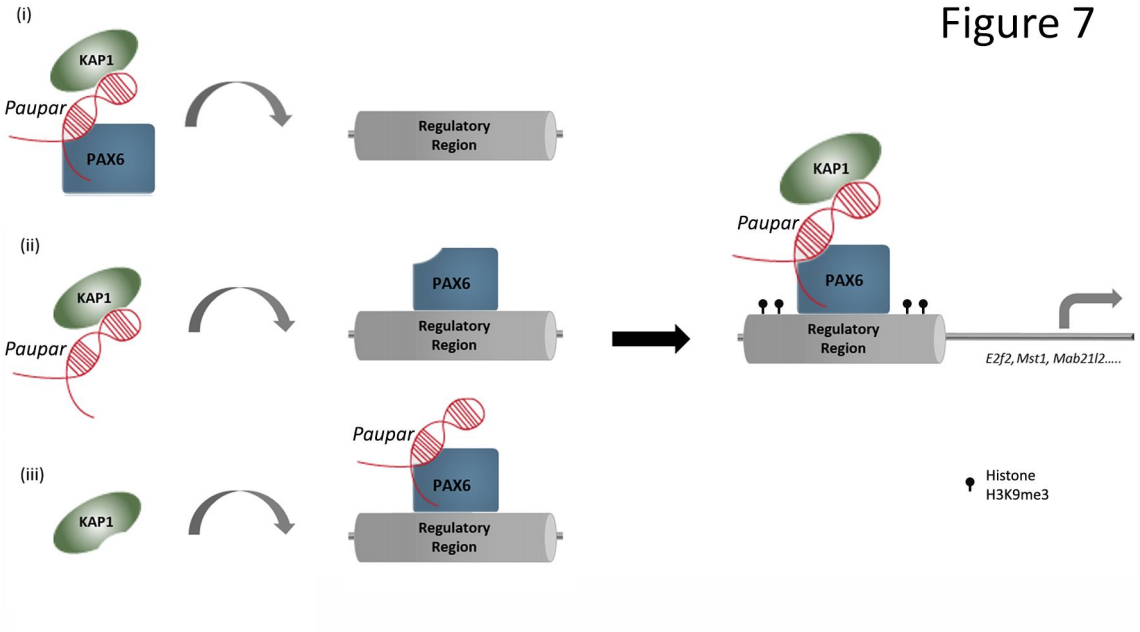
(i)
KAP1
Paupar
PAX6
Regulatory Region
(ii)
KAP1
Paupar
PAX6
Regulatory Region
(iii)
KAP1
Paupar
PAX6
Regulatory Region
KAP1
Paupar
PAX6
Regulatory Region
E2f2, Mst1, Mab21l2.....
Histone H3K9me3

Supplemental Figure S1

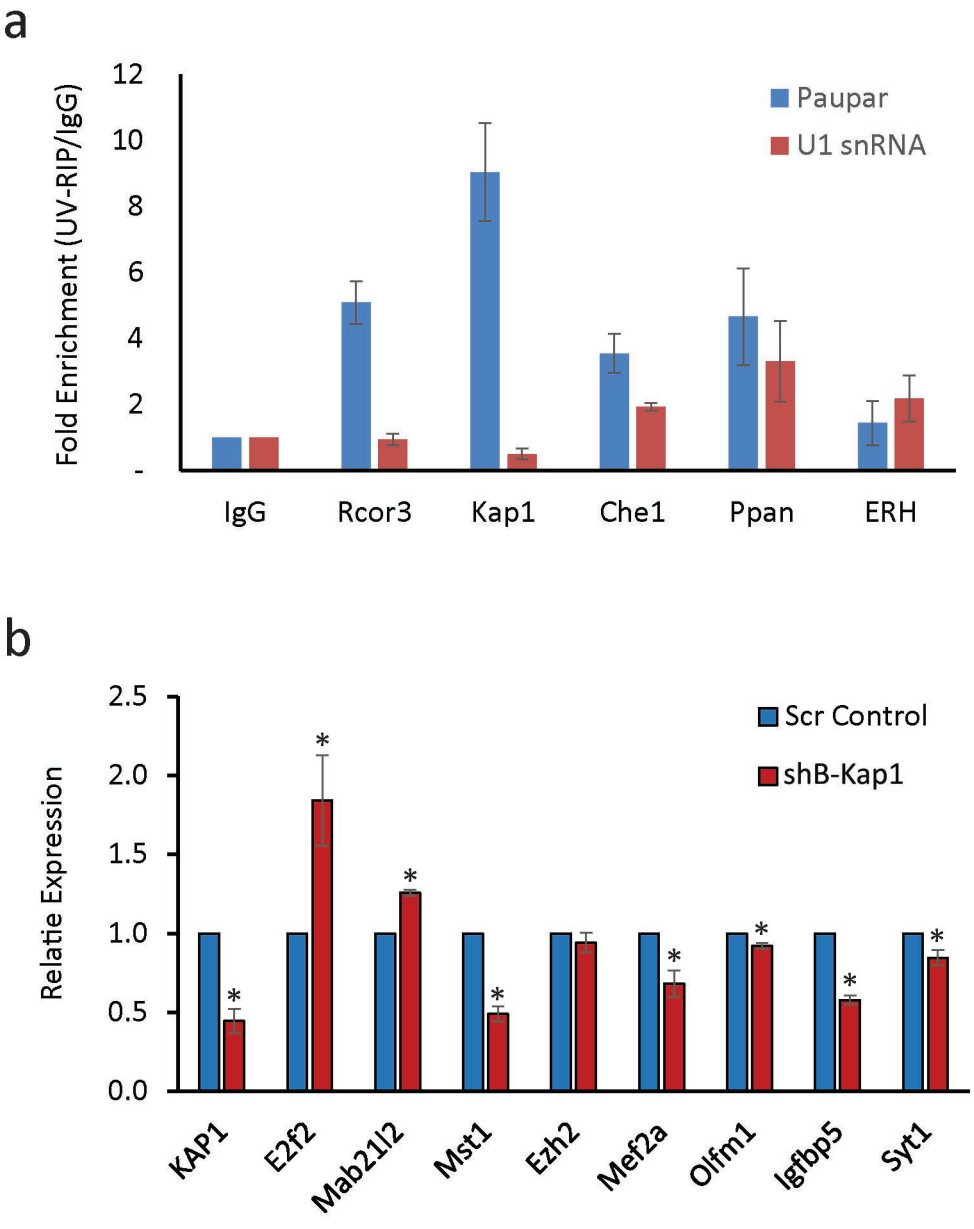

Supplemental Figure S2

a

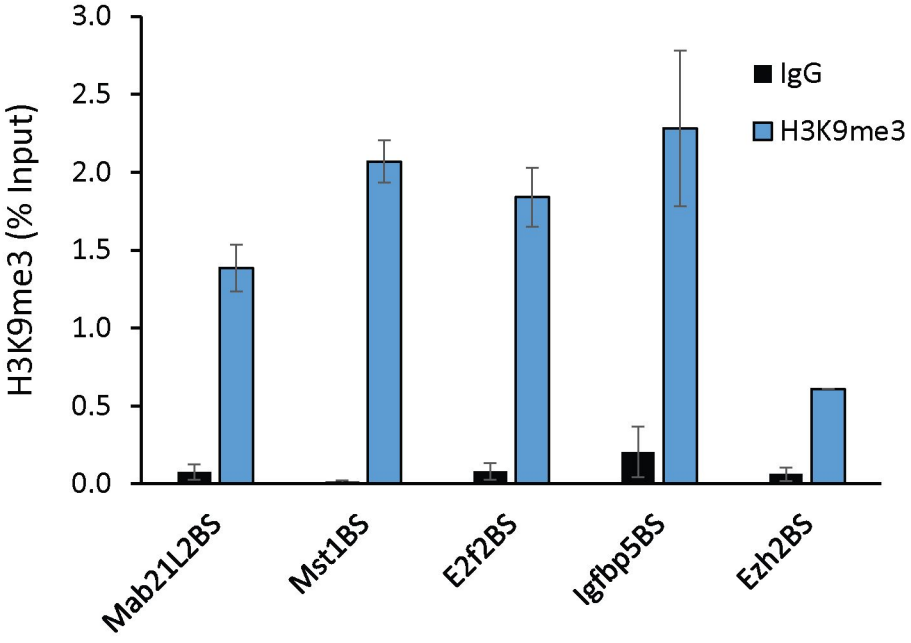

Supplemental Figure S3

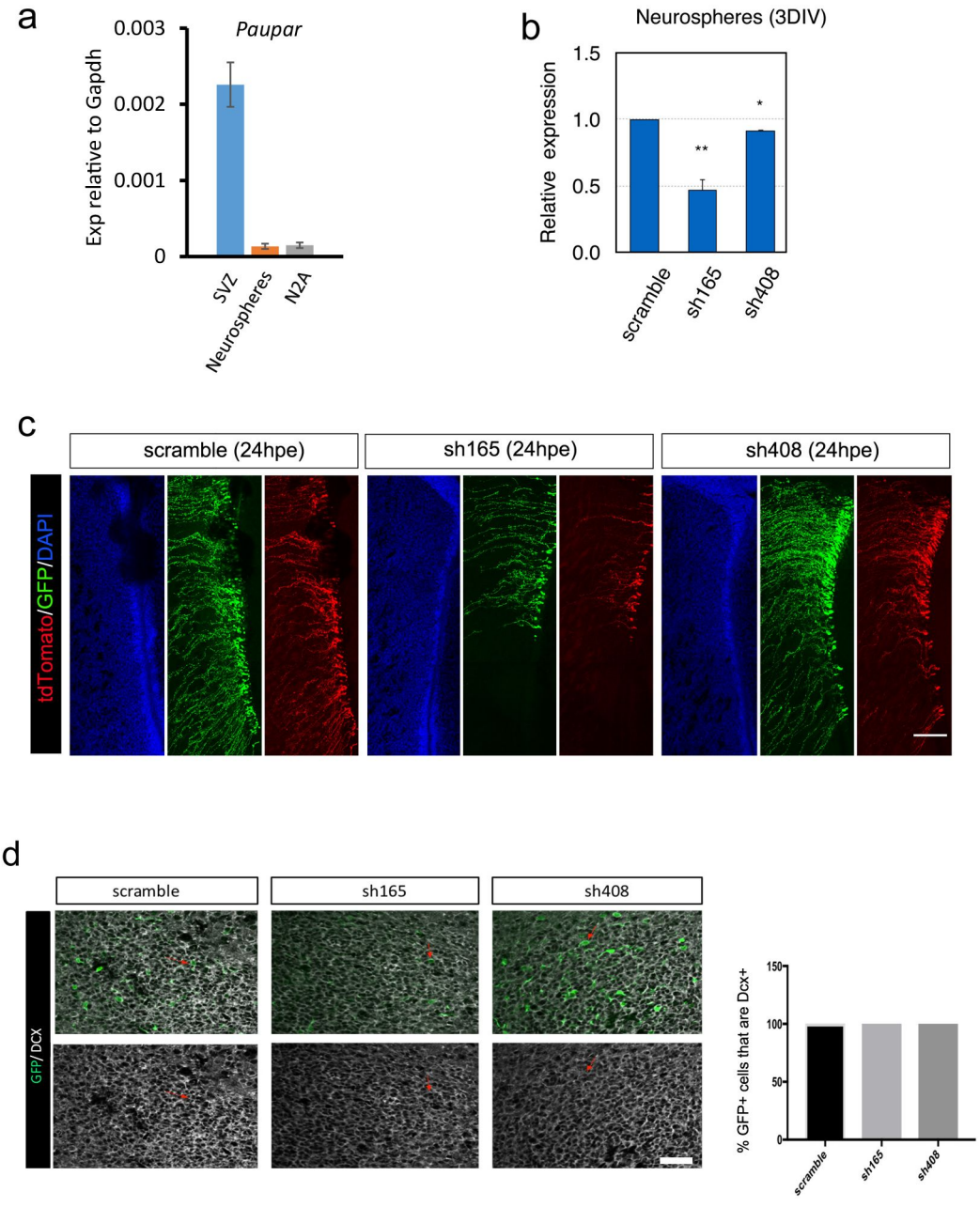

Supplemental Figure S4